Sub-Riemannian Geometry in Image Processing and Modelling of Human Visual System

Alexey Mashtakov

Program Systems Institute of RAS

Based on joint works with
R. Duits, Yu. Sachkov, G. Citti, A. Sarti, A. Popov
E. Bekkers, G. Sanguinetti, A. Ardentov, B. Franceschiello
I. Beschastnyi, A. Ghosh and T.C.J. Dela Haije

Scientific Heritage of Sergei A. Chaplygin
Nonholonomic Mechanics, Vortex Structures and Hydrodynamics
Cheboksary, Russia, 06.06.2019

SR geodesics on Lie Groups in Image Processing

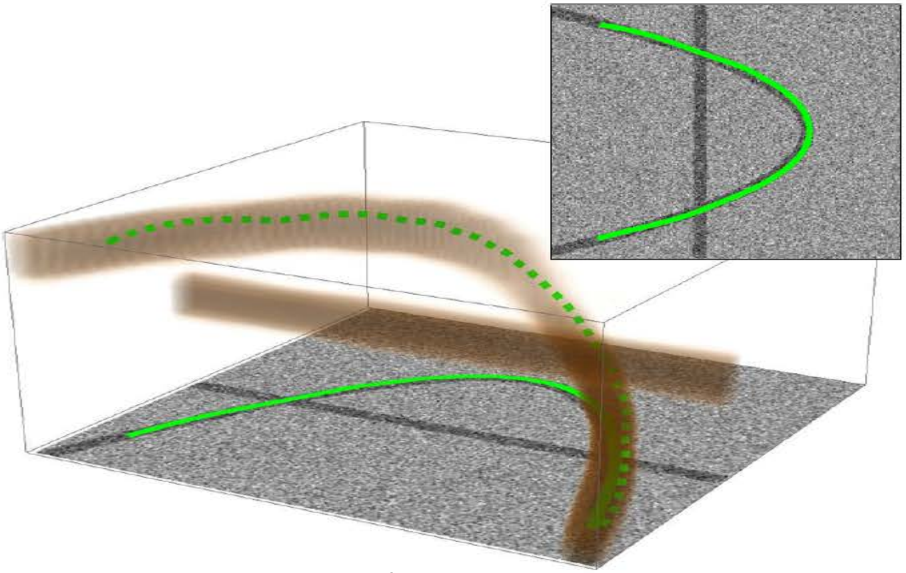

Crossing structures are disentangled

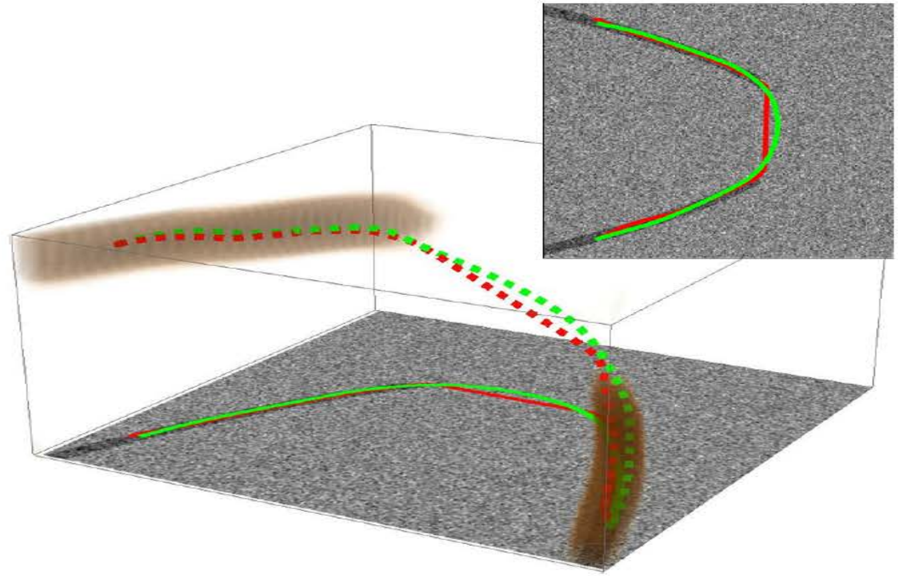

Reconstruction of corrupted contours based on model of human vision

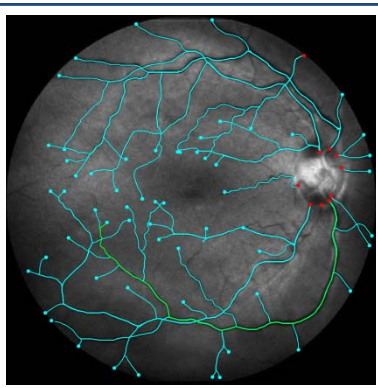

SE(2)

Applications in medical image analysis

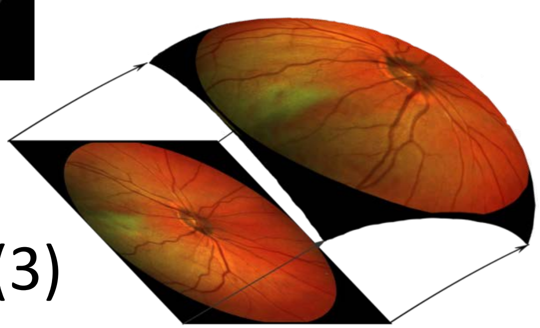

SO(3)

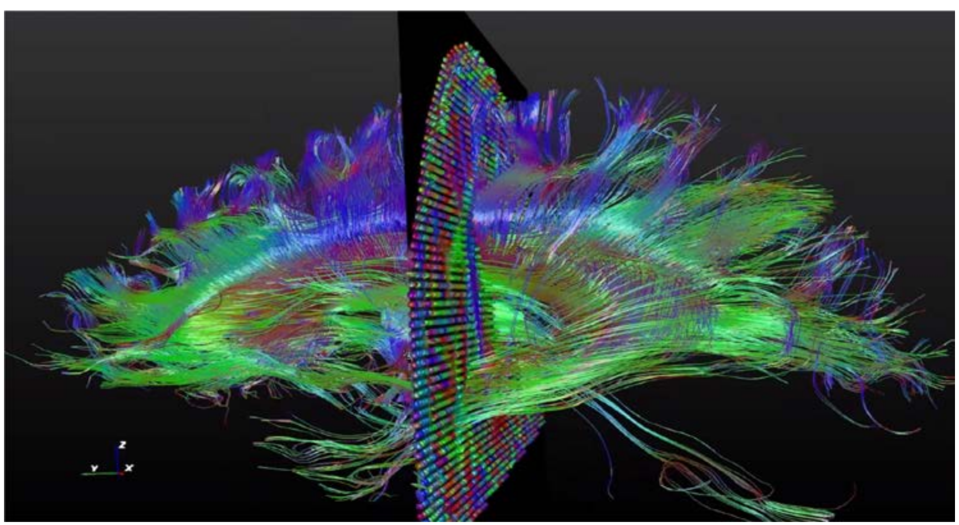

SE(3)

Left-invariant sub-Riemannian structures

- G – Lie group, e – unit element
  $\Delta \subset TG$ – left invariant subbundle of tangent bundle,
  $\mathcal{G}$ – left-invariant inner product in Δ.

- $\gamma : [0,T] \to G$ – horizontal (i.e. admissible) curve if

$$\dot\gamma(t) \in \Delta_{\gamma(t)} \text{ for a.e. } t \in [0,T].$$

SR length minimizers are horizontal curves γ that have minimum length

$$l(\gamma) = \int_0^T \sqrt{\mathcal{G}(\dot\gamma(t), \dot\gamma(t))}\, dt \to \min.$$

- Left-invariant contact sub-Riemannian structure on $d(d+1)/2$ Lie group:

$$(G, \Delta, \mathcal{G}), \ \Delta = \operatorname{span}(\mathcal{A}_1, \dots, \mathcal{A}_d), \ \mathcal{G}(\mathcal{A}_i, \mathcal{A}_j) = \delta_{ij}.$$

Here $\mathcal{A}_1, \dots, \mathcal{A}_d$ are left-invariant vector fields on G, s.t.

$$\Delta + [\Delta, \Delta] = TG.$$

Optimal Control Problem: ODE-based Approach

- Optimal Control Problem

$$\dot\gamma(t) = u_1(t)\ \mathcal{A}_1|_{\gamma(t)} + \ldots + u_d(t)\ \mathcal{A}_d|_{\gamma(t)}$$
$$\gamma(0) = e, \qquad \gamma(T) = g_1$$
$$l(\gamma) = \int_0^T \sqrt{u_1(t)^2 + \ldots + u_d(t)^2}\, dt \to \min$$
$$(u_1(t), \ldots, u_d(t)) \in \mathbb{R}^d,$$

- Pontryagin Maximum Principle: the Hamiltonian system

$$\dot\lambda = \vec{H}(\lambda), \quad \lambda \in T^*G$$

- Exponential mapping:

$$\mathrm{Exp} : (\lambda_0, t) \mapsto \gamma(t)$$

Optimality of Extremal Trajectories

- Short arcs of extremal trajectories γ are optimal
- Cut time along γ:

$$t_{cut} = \sup\{\tau > 0 \mid \gamma(t) \text{ is optimal for } t \in [0, \tau]\}.$$

- Maxwell time t_{max}:

$$\exists\ \tilde{\gamma} \not\equiv \gamma\ :\ \begin{cases} \gamma(0) = \tilde{\gamma}(0), \\ \gamma(t_{max}) = \tilde{\gamma}(t_{max}) \end{cases}$$

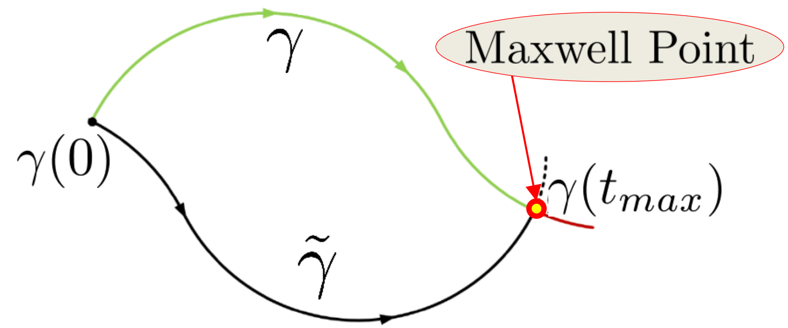

- Conjugate time t_{conj}:

  Conjugate point – critical value of Exp:

$$\frac{\partial\,\mathrm{Exp}}{\partial(\lambda, t)}(\lambda_0, t_{conj}) = 0.$$

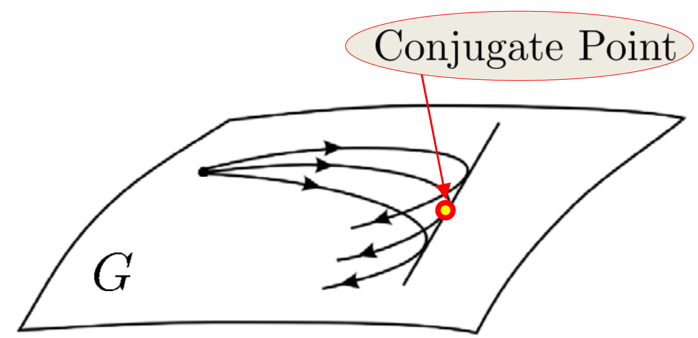

- Upper bound on cut time:

$$t_{cut} \leq \min(t_{max}, t_{conj}).$$

Sub-Riemannian Wave Front

$$W(T) = \{\text{Exp}(\lambda_0, T) | \lambda_0 \in T_e^* G, \text{H}(\lambda_0) = \tfrac{1}{2}\}.$$

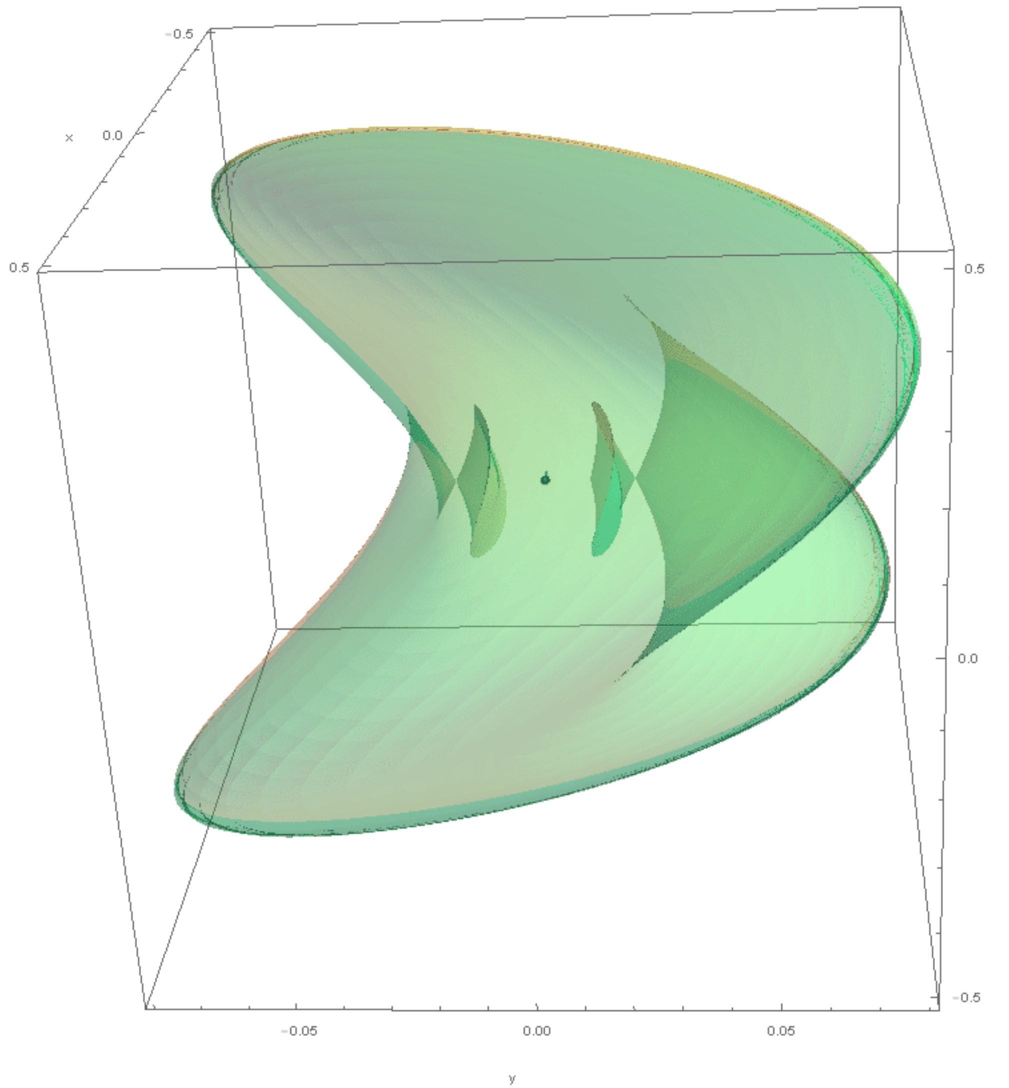

$\lambda_0 = (\nu_0, c_0)$

Varying t
$\Rightarrow$
one geodesic

Sub-Riemannian Wave Front

$$W(T) = \{\mathrm{Exp}(\lambda_0, T) | \lambda_0 \in T_e^*G, \mathrm{H}(\lambda_0) = \tfrac{1}{2}\}.$$

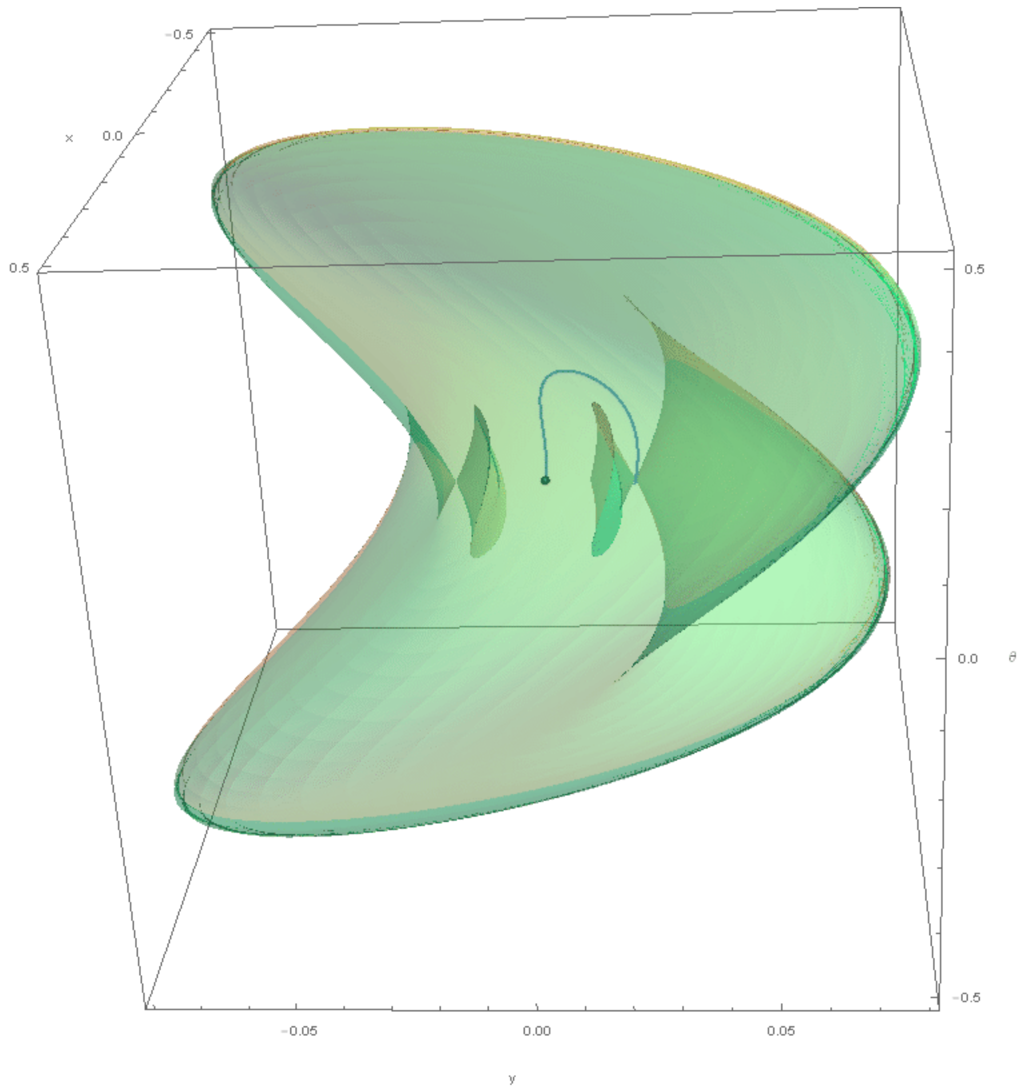

$\lambda_0 = (\nu_0, c_0)$

$t \in [0, T]$
Varying ν_0
$\Rightarrow$ family of geodesics

Sub-Riemannian Wave Front

$$W(T) = \{\mathrm{Exp}(\lambda_0, T) | \lambda_0 \in T_e^* G, \mathrm{H}(\lambda_0) = \tfrac{1}{2}\}.$$

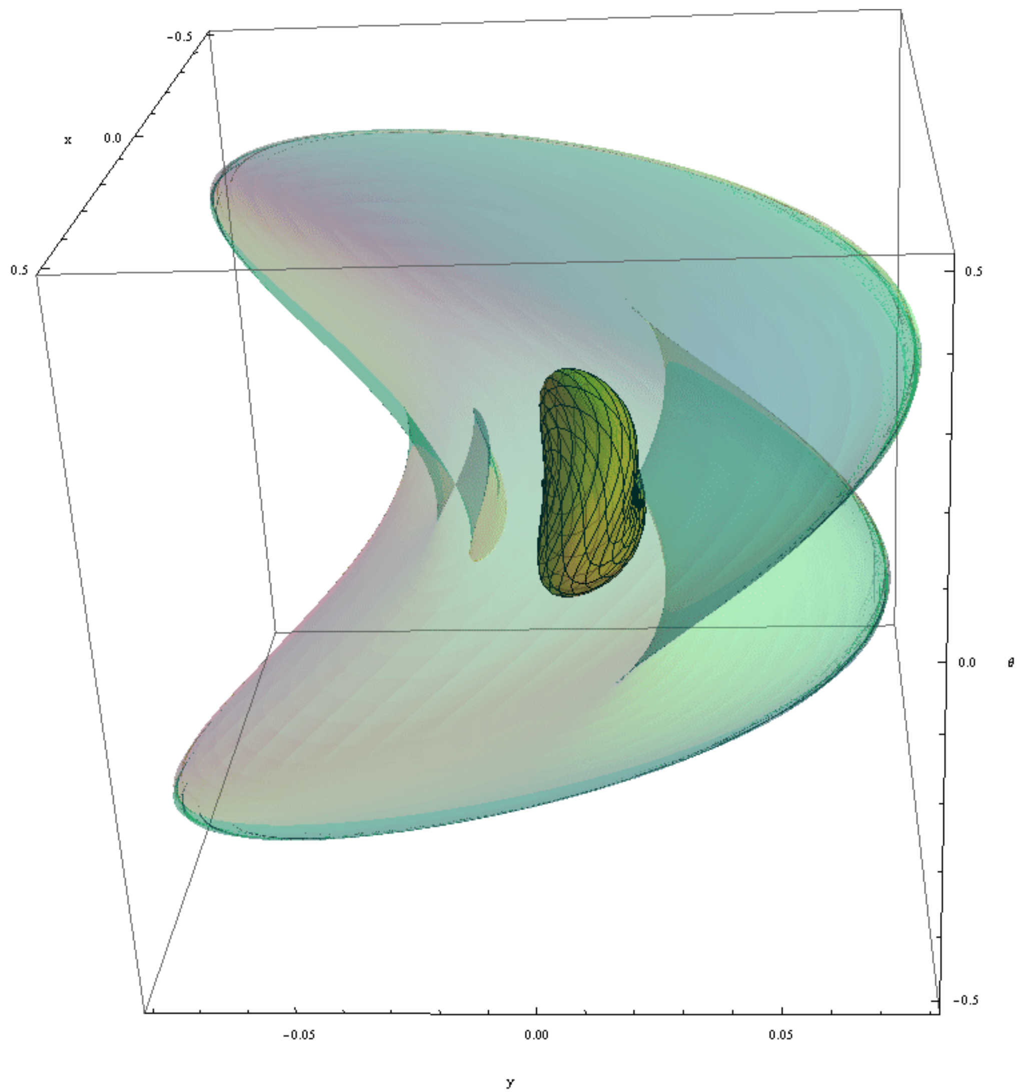

$$\lambda_0 = (\nu_0, c_0)$$

$$t \in [0, T]$$

$$2\nu_0 \in S^1$$

Varying c_0

$\Rightarrow$

whole family of geodesics

Self intersection of Sub-Riemannian Wave Front

General case: astroidal shape of conjugate locus

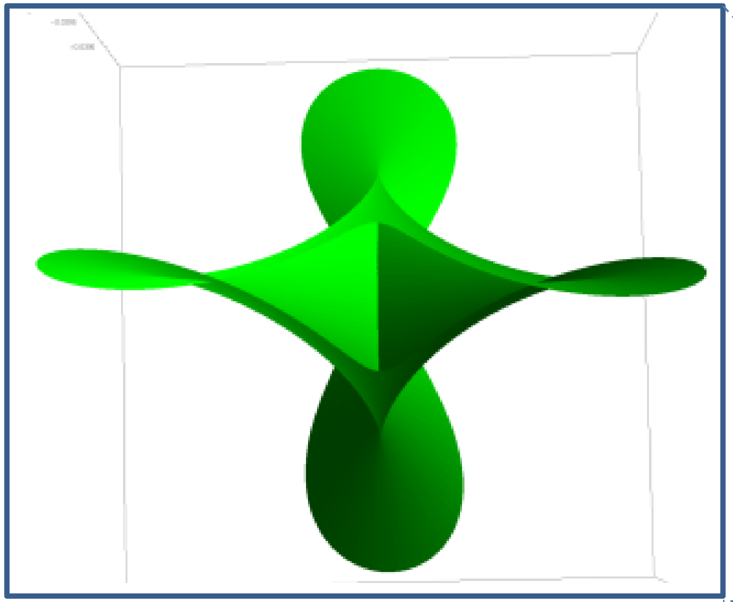

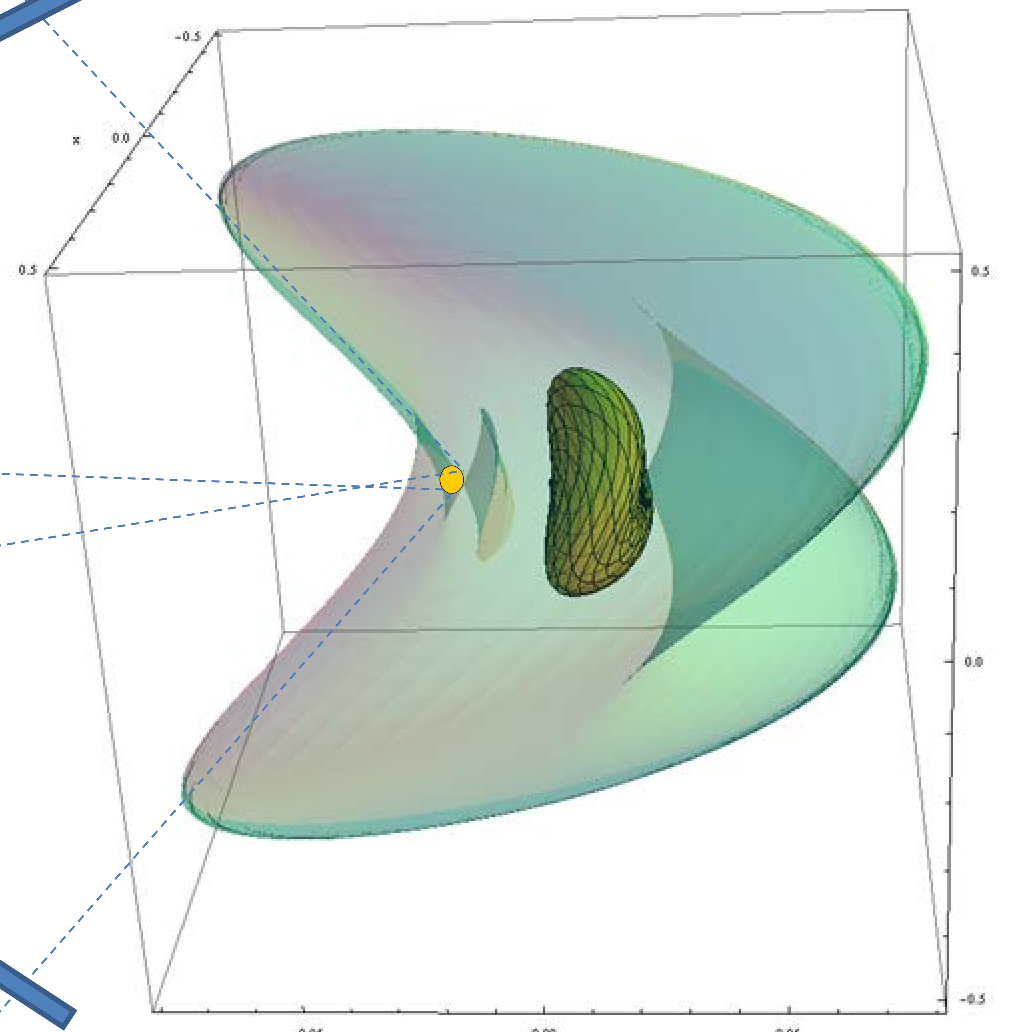

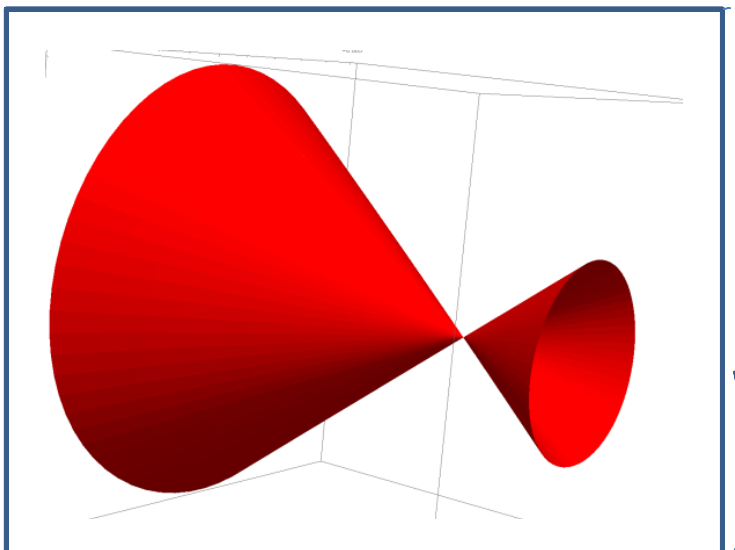

Special case with rotational symmetry

A.Agrachev, Exponential mappings for contact sub-Riemannian structures. JDCS, 1996.
H. Chakir, J.P. Gauthier and I. Kupka, Small Subriemannian Balls on R3. JDCS, 1996.

Sub-Riemannian Sphere

$$S(T) = \{\mathrm{Exp}(\lambda_0, T) | \lambda_0 \in T_e^*G, \mathrm{H}(\lambda_0) = \frac{1}{2}, t_{cut}(\lambda_0) \geq T\}.$$

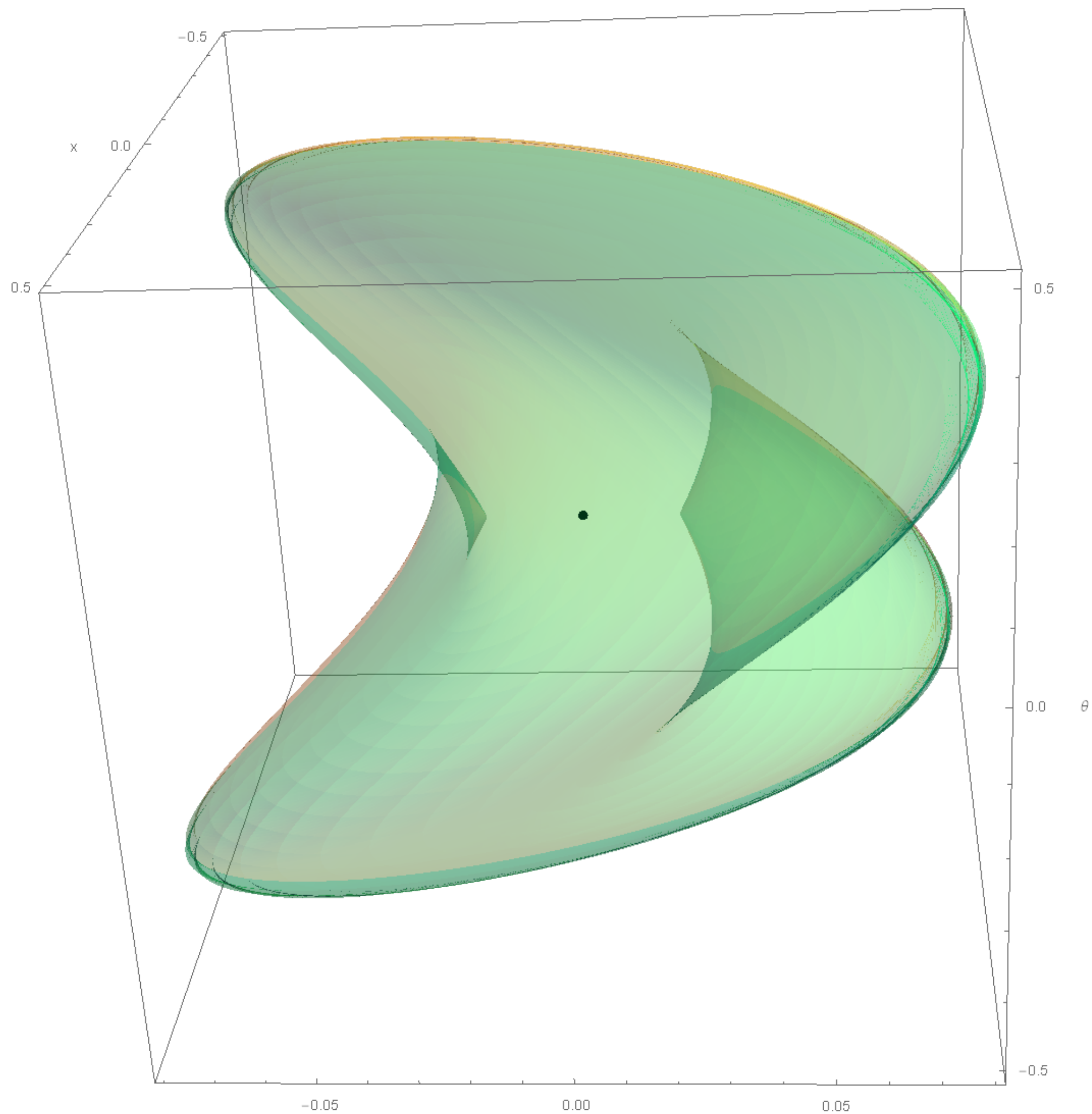

Sub-Riemannian Length Minimizers

Problem Statement.

$$\dot{\gamma} = \sum_{i=1}^{d} u_i \mathcal{A}_i, \quad \gamma(0) = e,\ \gamma(T) = g, \quad l(\gamma) = \int_0^T \mathcal{C}(\gamma(t)) \sqrt{\sum_{i=1}^{d} u_i^2(t)}\, dt \to \min$$

Theorem. Let $\mathcal{W}(g)$ be a viscosity solution of eikonal system

$$\begin{cases} \sum_{i=1}^{d} (\mathcal{A}_i|_g (\mathcal{W}))^2 = \mathcal{C}^2(g), \ \text{for } g \neq e, \\ \mathcal{W}(e) = 0. \end{cases}$$

Then

- $\mathcal{W}(g) = d(e, g)$ is the SR distance map;
- $\mathcal{S}_t = \{g \in G \mid \mathcal{W}(g) = t\}$ are SR-spheres $\mathrm{S}(t)$ of radius t;
- SR-minimizer $\gamma(t)$ connecting e to g is given by $\gamma(t) = \gamma_b(\mathcal{W}(g) - t)$, where $\gamma_b(t)$ is found by integration for $t \in [0, \mathcal{W}(g)]$

$$\dot{\gamma}_b(t) = -u_1(t)\mathcal{A}_1|_{\gamma_b(t)} - \ldots - u_d(t)\,\mathcal{A}_d|_{\gamma_b(t)}, \qquad \gamma_b(0) = g,$$

where $u_i(t) = \frac{\mathcal{A}_i|_{\gamma_b(t)}(\mathcal{W})}{\mathcal{C}^2(\gamma_b(t))}$, $i = 1, \ldots, d$.

Brain Inspired Methods in Computer Vision

Perception of Visual Information by Human Brain

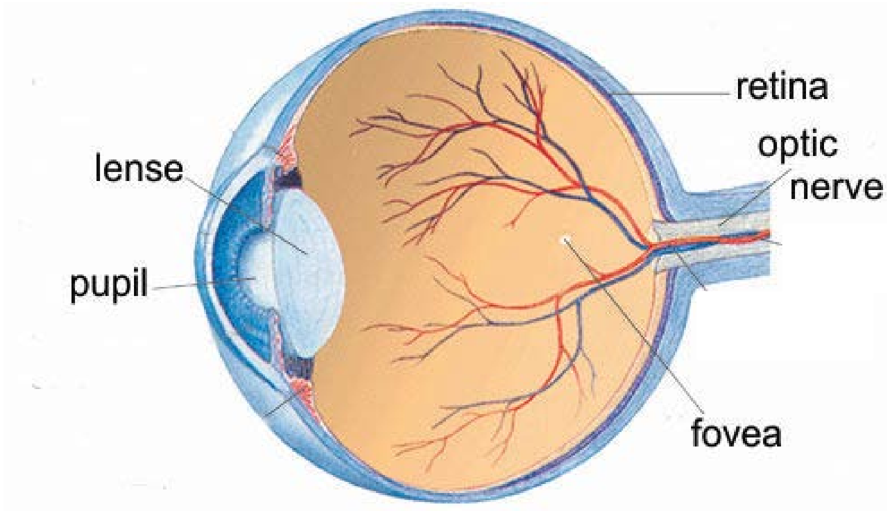

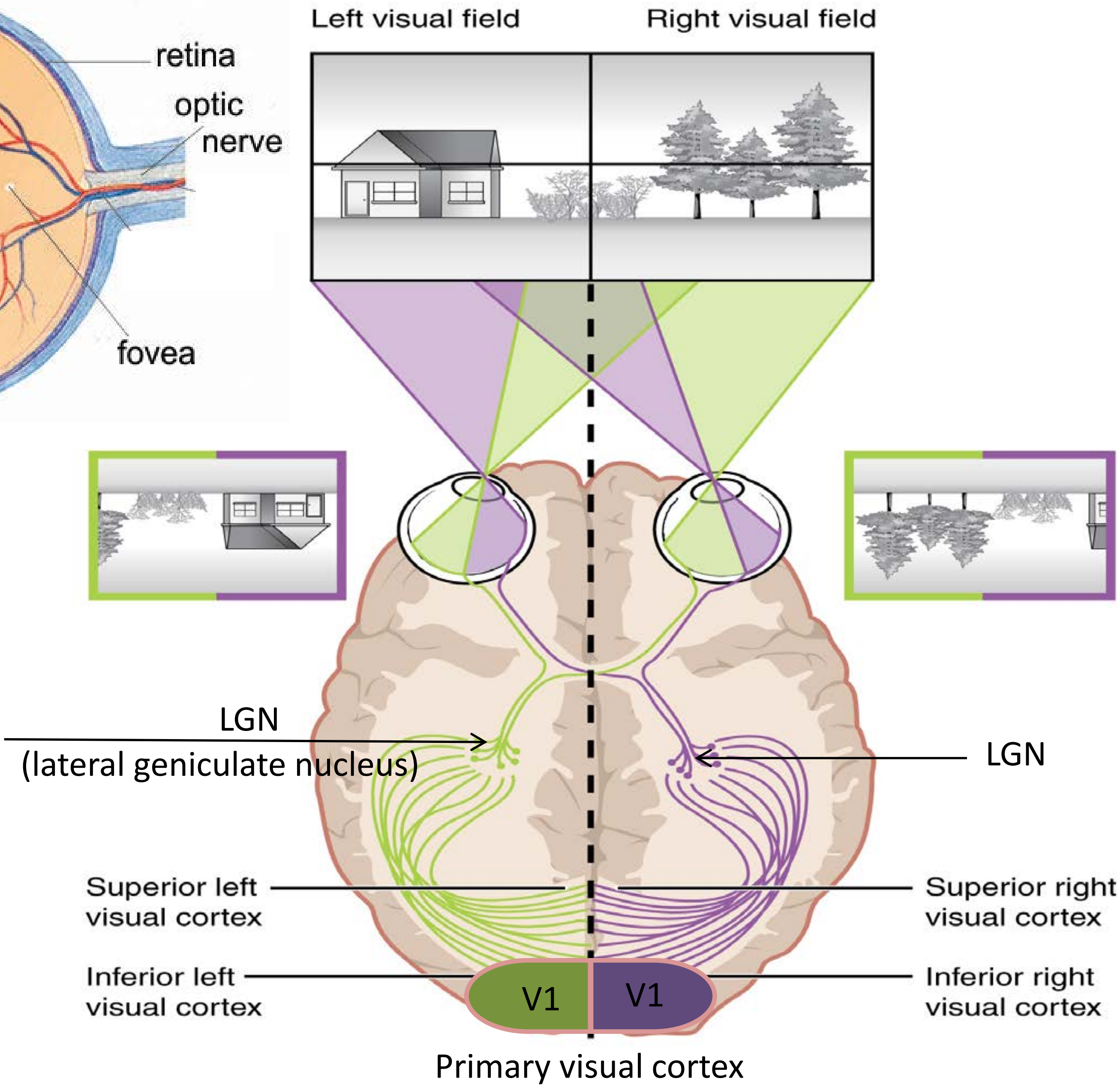

A Model of the Primary Visual Cortex V1

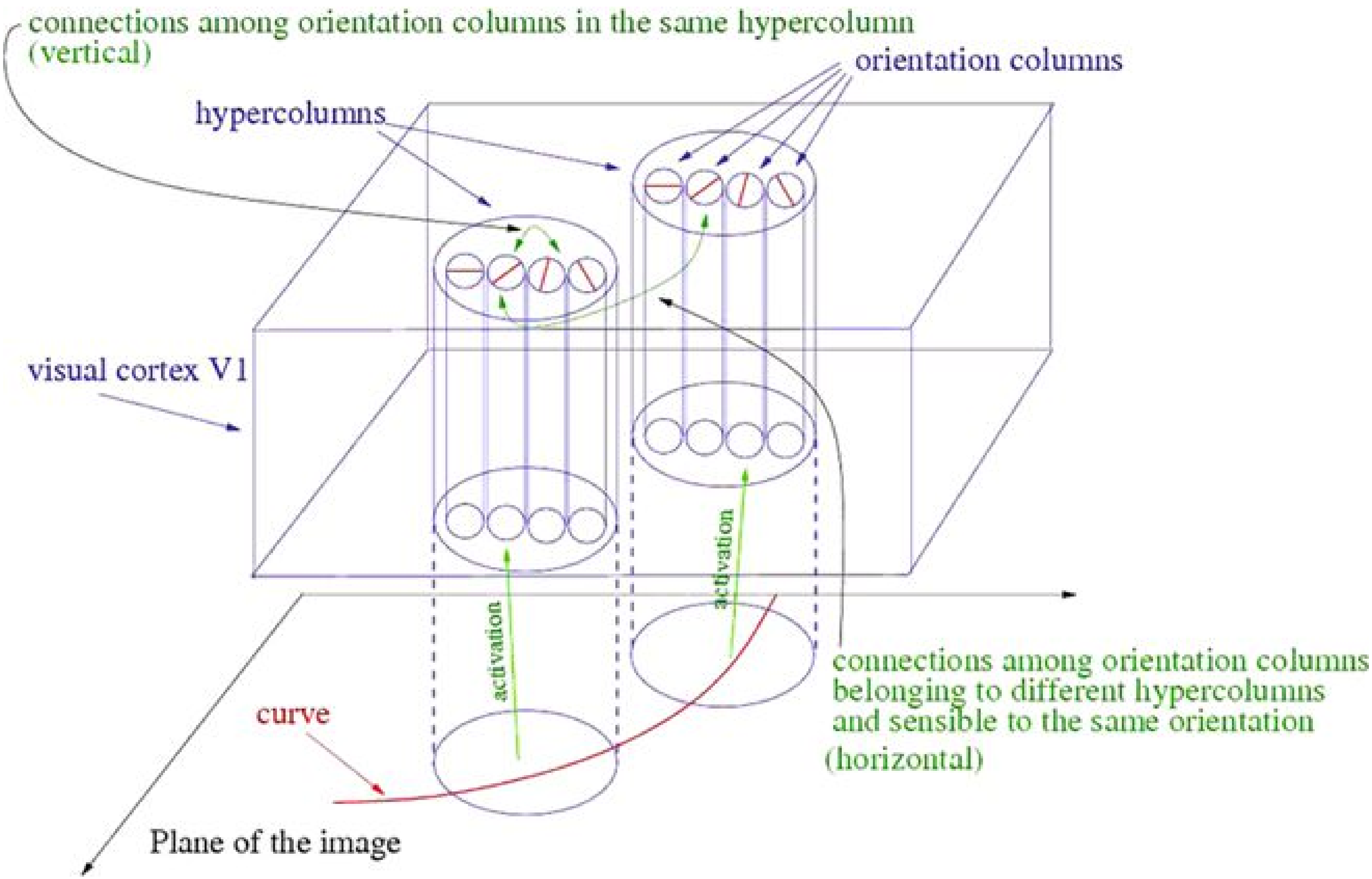

Replicated from R. Duits, U. Boscain, F. Rossi, Y. Sachkov,
Association Fields via Cuspless Sub-Riemannian Geodesics in SE(2), JMIV, 2013.

Cortical Based Model of Perceptual Completion

- D.H. Hubel and T.N. Wiesel, Receptive fields of single neurones in the cat's striate cortex, 1959. Nobel prize in 1981.
- Sub-Riemanian structures in neurogeometry of the vision:
  - J. Petitot, The neurogeometry of pinwheels as a sub-Riemannian contact structure, 2003. (Heisenberg group.)
  - G. Citti and A. Sarti, A Cortical Based Model of Perceptual Completion in the Roto-Translation Space, 2006. ($SE(2)$ group.)
- Variational principle: recovered arc has minimal length in the space (x, y, θ):

$$\int \sqrt{\xi^2\left(\dot{x}^2+\dot{y}^2\right)+\dot{\theta}^2}dt \to \min, \text{ under constraint } \dot{\theta} = \arg\left(\dot{x}+\mathrm{i}\ \dot{y}\right)$$

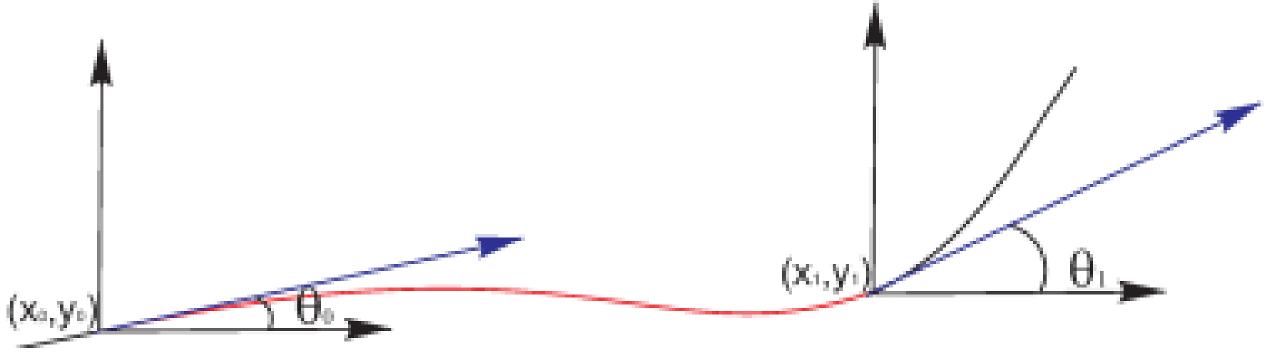

Detection of salient curves in images

Analysis of Images of the Retina

Diabetic retinopathy --- one of the main causes of blindness.
Epidemic forms: 10% people in China suffer from DR.
Patients are found early --> treatment is well possible.
Early warning --- leakage and malformation of blood vessels.
The retina --- excellent view on the microvasculature of the brain.

Healthy retina

Diabetes Retinopathy with tortuous vessels

Geodesic Methods in Computer Vision

Image

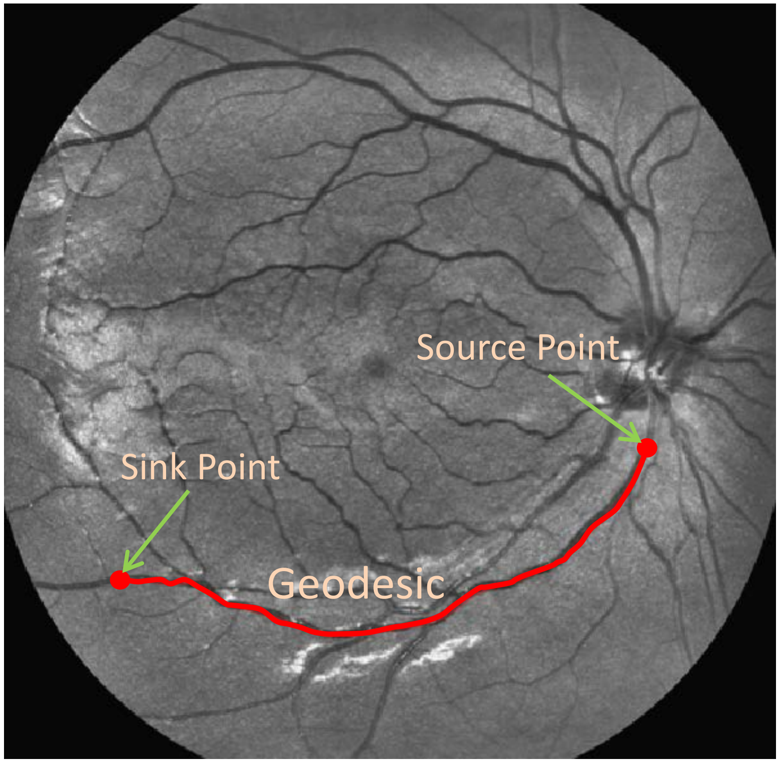

Distance from source point

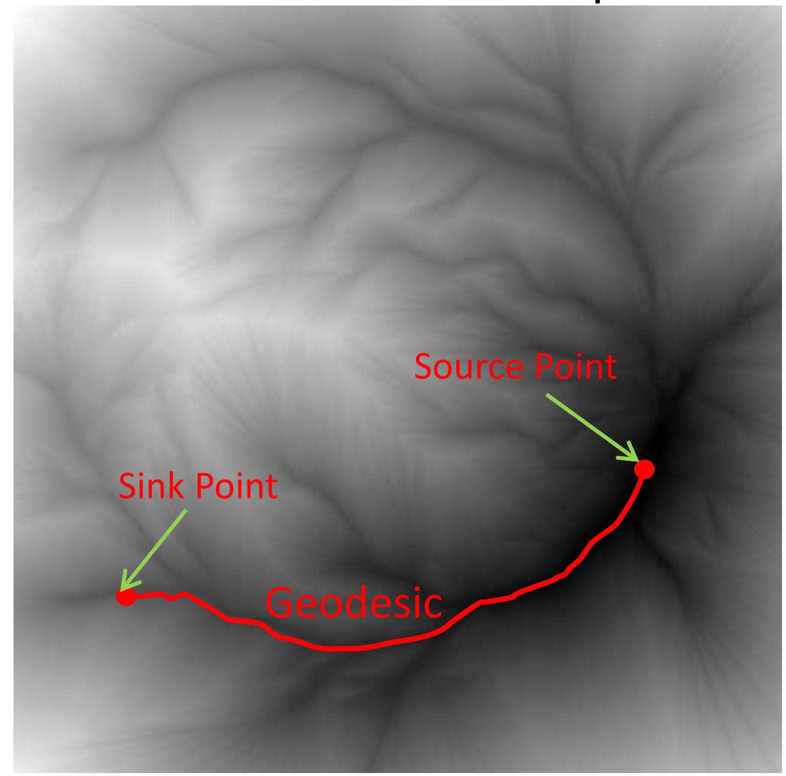

Tracking of salient lines via data-driven minimal paths (or geodesics).

Data-driven Geodesic – curve that minimizes length functional weighted by external cost (function with high values at image locations with high curve saliency).

Fast Marching method to compute geodesics:

1) Computation of distance map from source point,
2) Geodesic via steepest decent on distance map.

Tracking of Lines in Flat Images via Sub-Riemannian Geodesics in SE(2)

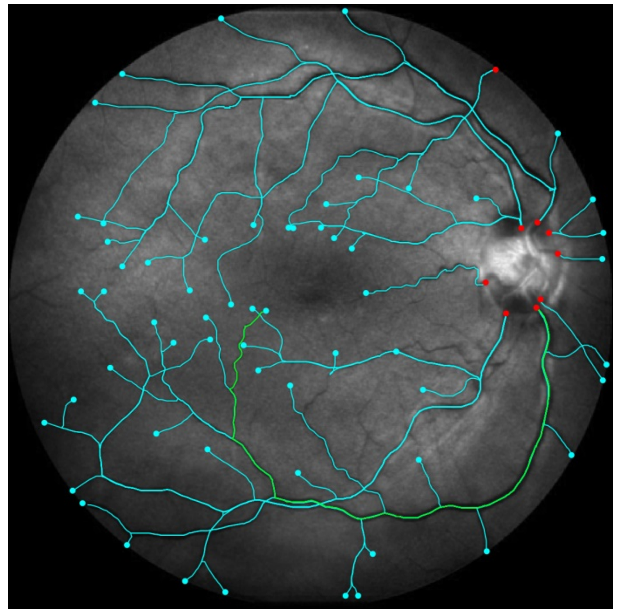

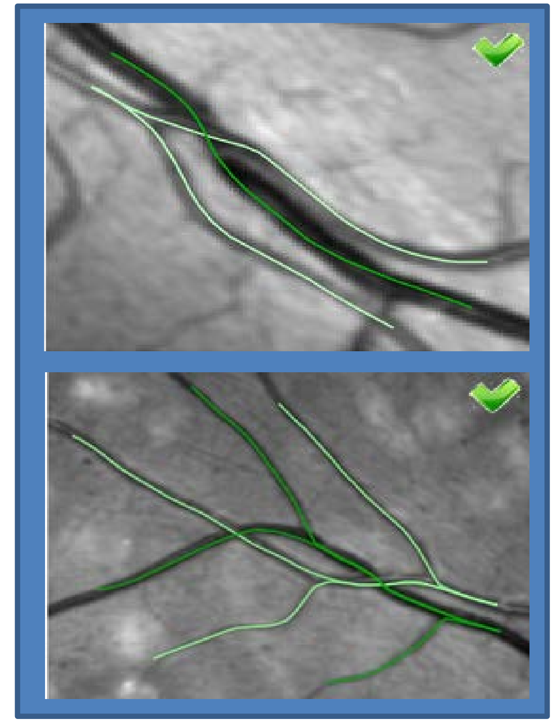

[1] E.J. Bekkers, R. Duits, A. Mashtakov and G.R. Sanguinetti, *Data-driven Sub-Riemannian Geodesics in* SE(2), Proc. SSVM, 2015.

[2] E.J. Bekkers, R. Duits, A. Mashtakov and G.R. Sanguinetti, *A PDE Approach to Data-driven Sub-Riemannian Geodesics in* SE(2), SIIMS, 2015.

[3] G. Sanguinetti, R. Duits, E. Bekkers, M. Janssen, A. Mashtakov, J-M. Mirebeau, *Sub-Riemannian Fast Marching in* SE(2), Proc. CIARP, 2015.

Comparison with Classical Methods

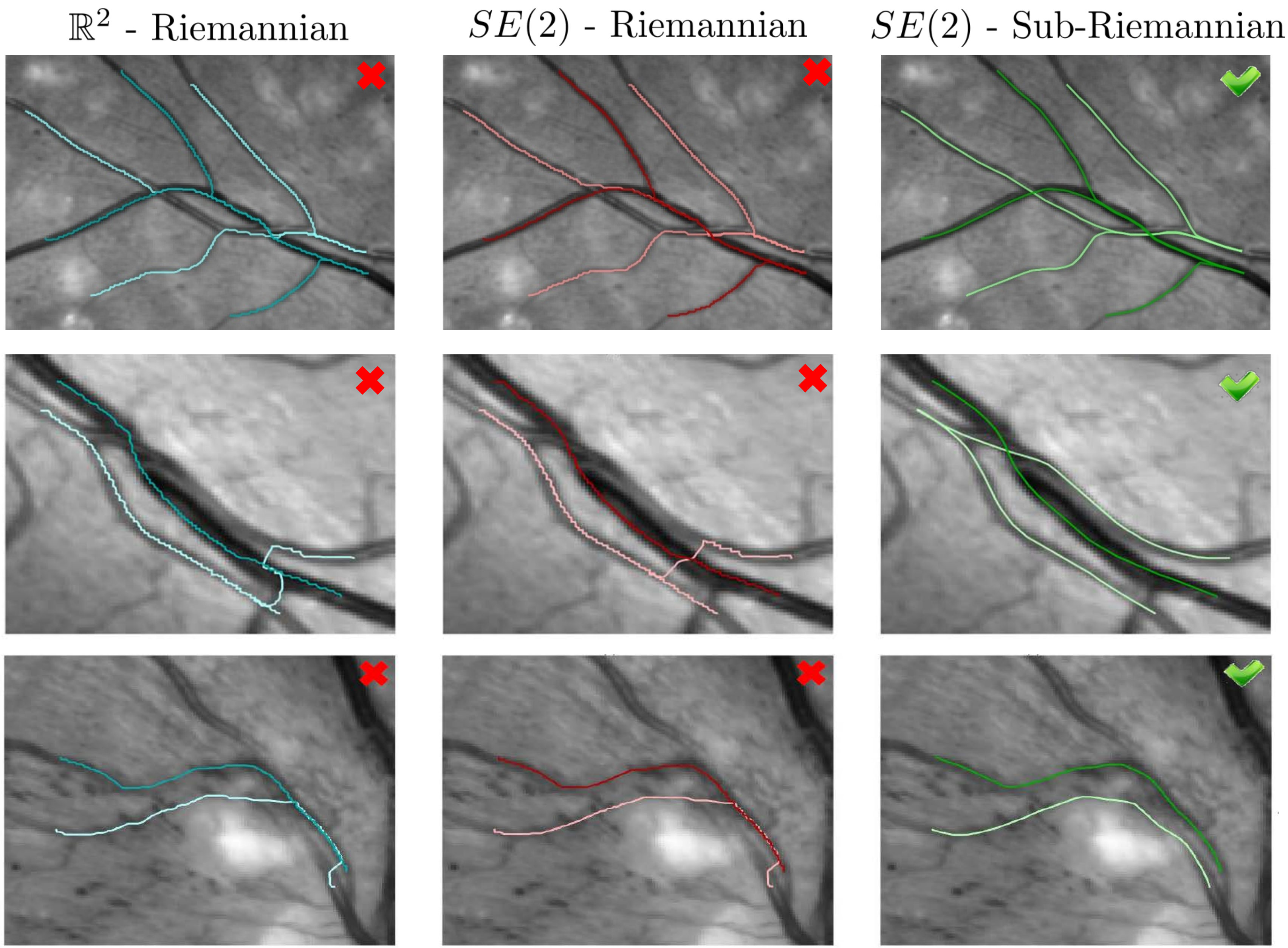

Numerical Verification for C=1

Converging to Exact Geodesics

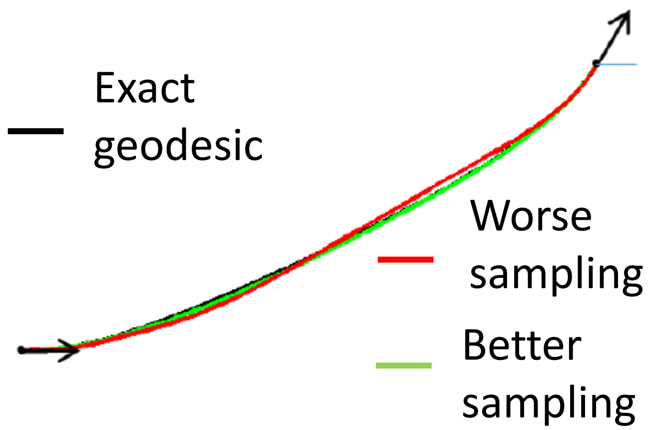

SR-sphere Numerically

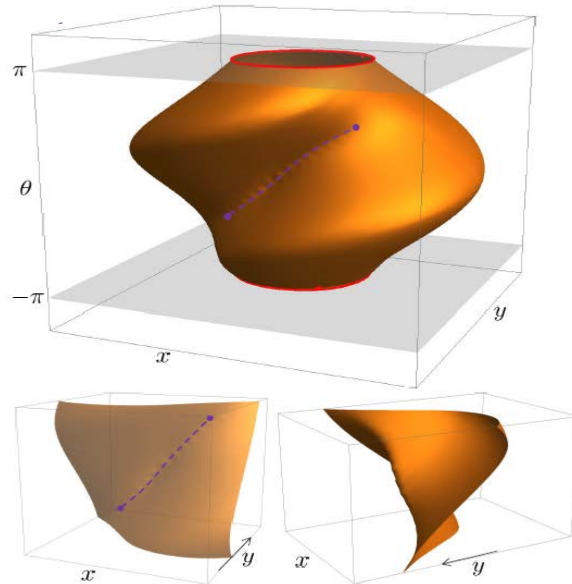

Exact Wavefront

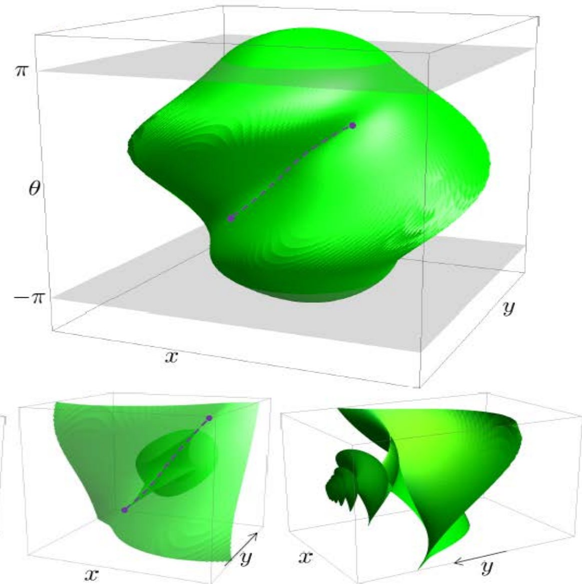

Max Absolute Error

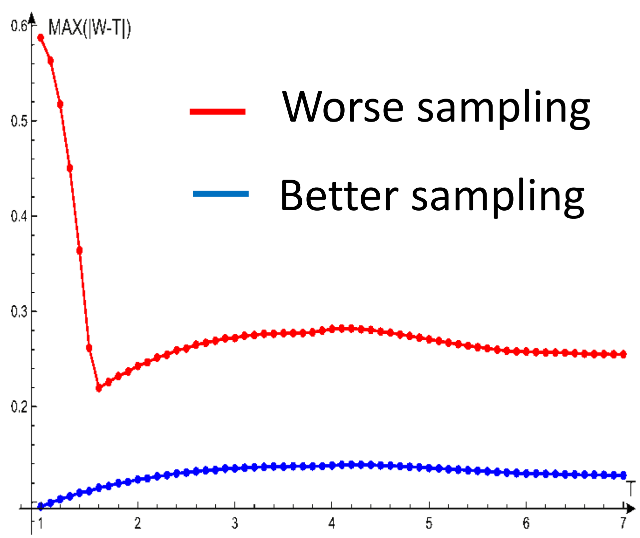

(T – radius of SR-sphere)

Maxwell Set Exact

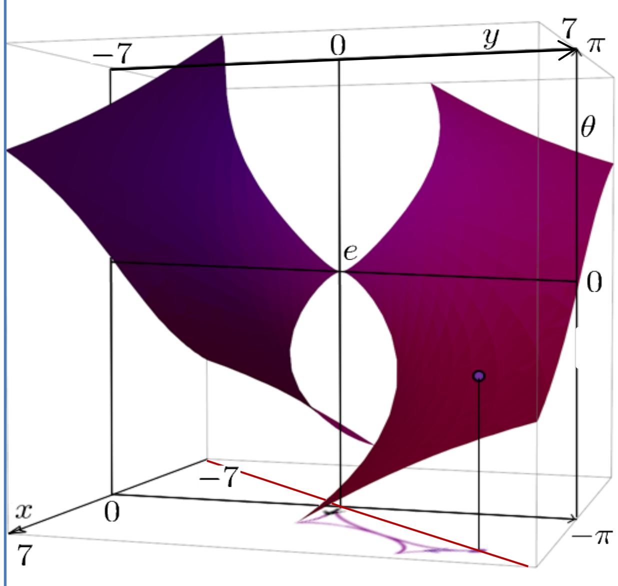

Maxwell Set Numerically

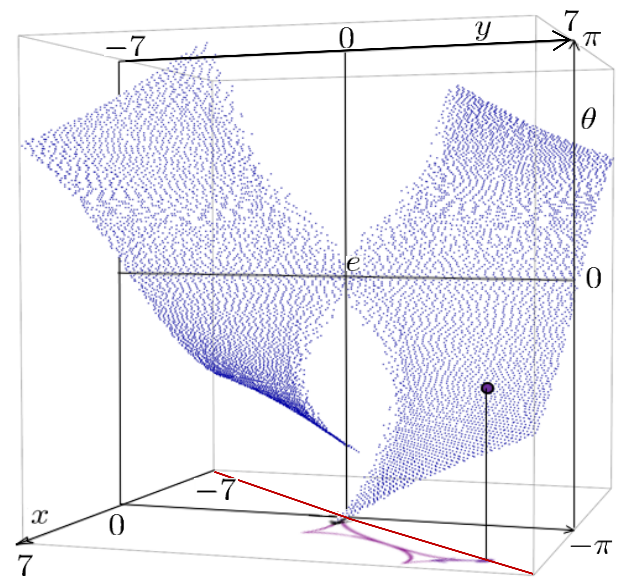

Tracking of Lines in Spherical Images via Sub-Riemannian Geodesics in SO(3)

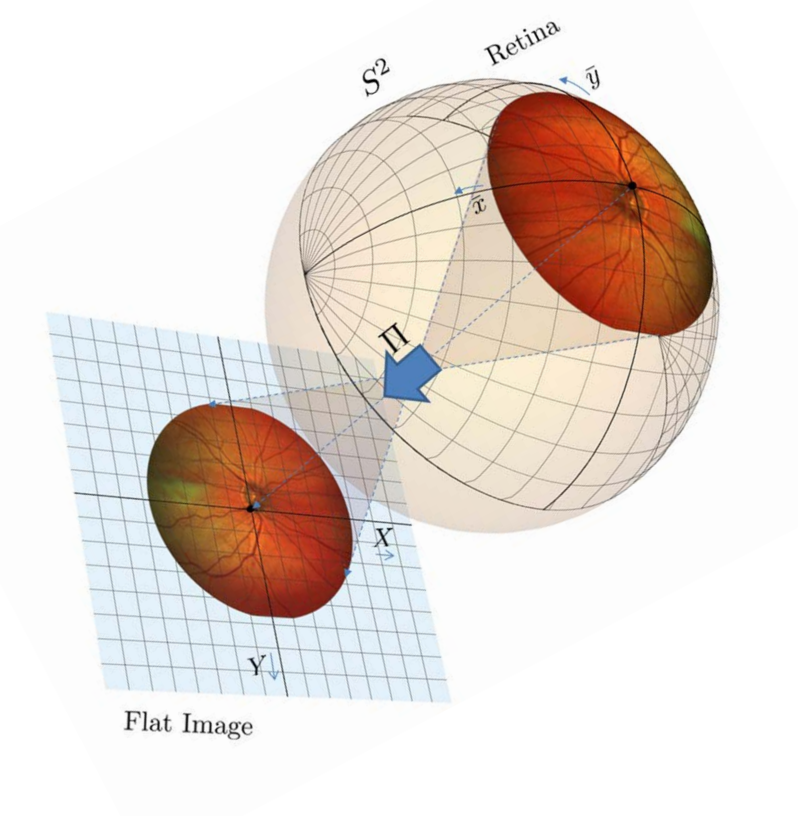

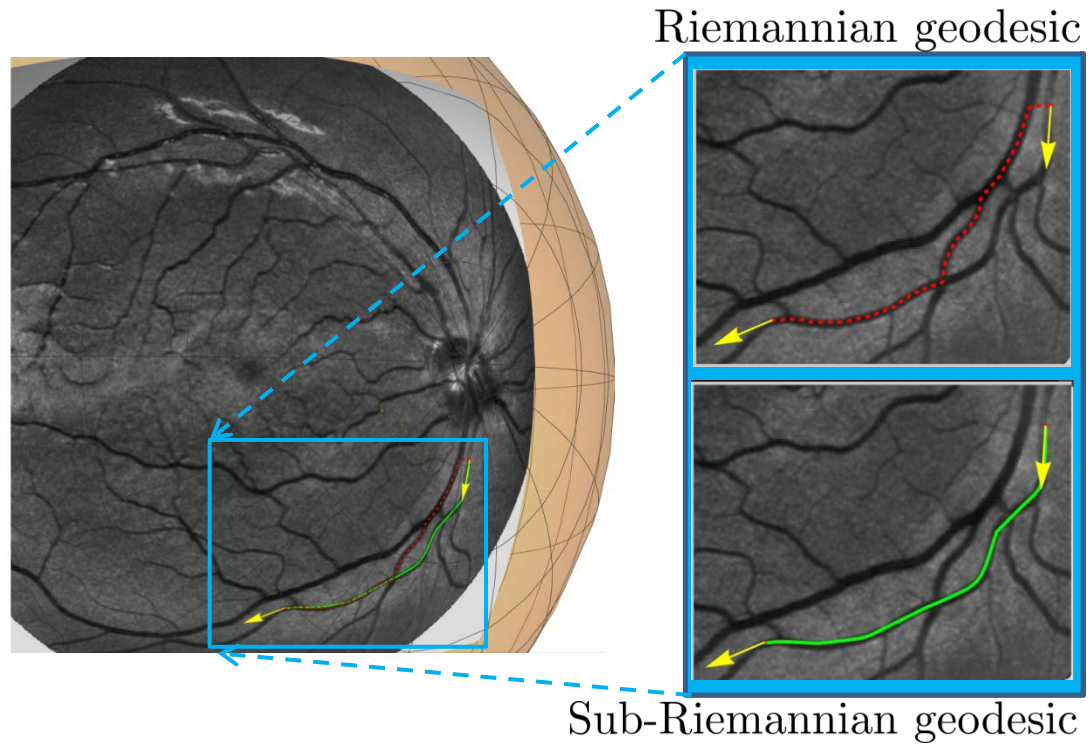

[**1**] A. Mashtakov, R. Duits, Yu. Sachkov, E.J. Bekkers, I. Beschastnyi, *Tracking of Lines in Spherical Images via Sub-Riemannian Geodesics in SO(3)*, JMIV, 2017.

[**2**] A.P. Mashtakov, R. Duits, Yu.L. Sachkov, E.J. Bekkers, I.Yu. Beschasnyi, *Sub-Riemannian Geodesics in SO(3) with Application to Vessel Tracking in Spherical Images of Retina*, Doklady Mathematics, 2017.

Vessel Curvature via Data-driven SR-geodesics on SO(3)

X_i - l.-i. v.f. on SO(3)

$\mathcal{A}_i$ - l.-i. v.f. on SE(2)

$\gamma^{SO(3)}$ -SO(3) geodesic

$\gamma^{SE(2)}$ - SE(2) geodesic

$\mathcal{W}$ - SR-distance
from source point

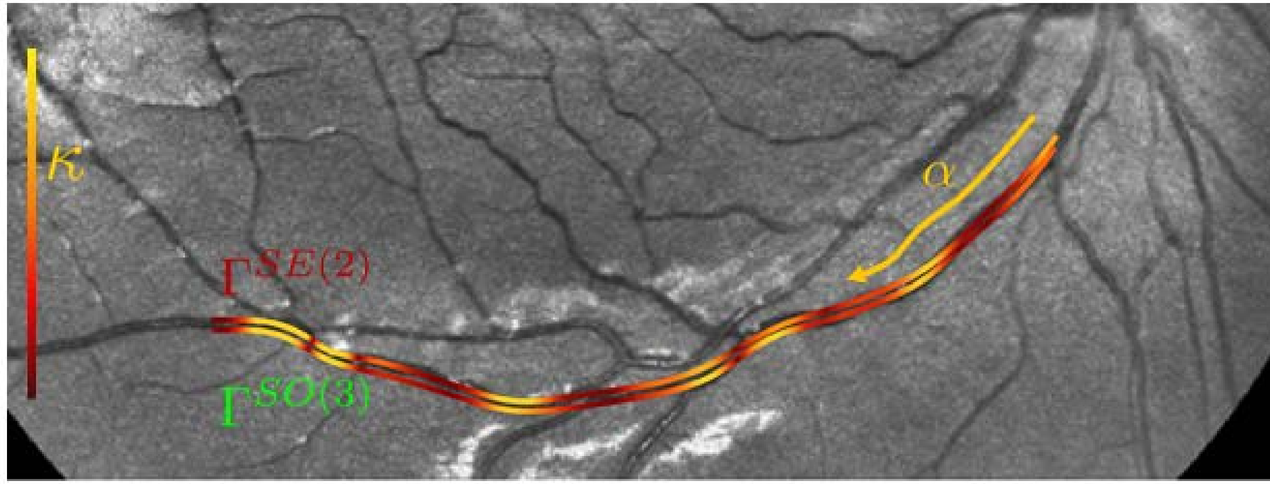

Geodesic curvature

$$\kappa_g^{SO(3)}(\cdot) = = -\xi^2 \frac{X_2|_{\gamma^{SO(3)}(\cdot)}(\mathcal{W}^{SO(3)})}{X_1|_{\gamma^{SO(3)}(\cdot)}(\mathcal{W}^{SO(3)})}$$

Plannar curvature

$$\kappa^{SE(2)}(\cdot) = = -\xi^2 \frac{\mathcal{A}_2|_{\gamma^{SE(2)}(\cdot)}(\mathcal{W}^{SE(2)})}{\mathcal{A}_1|_{\gamma^{SE(2)}(\cdot)}(\mathcal{W}^{SE(2)})}$$

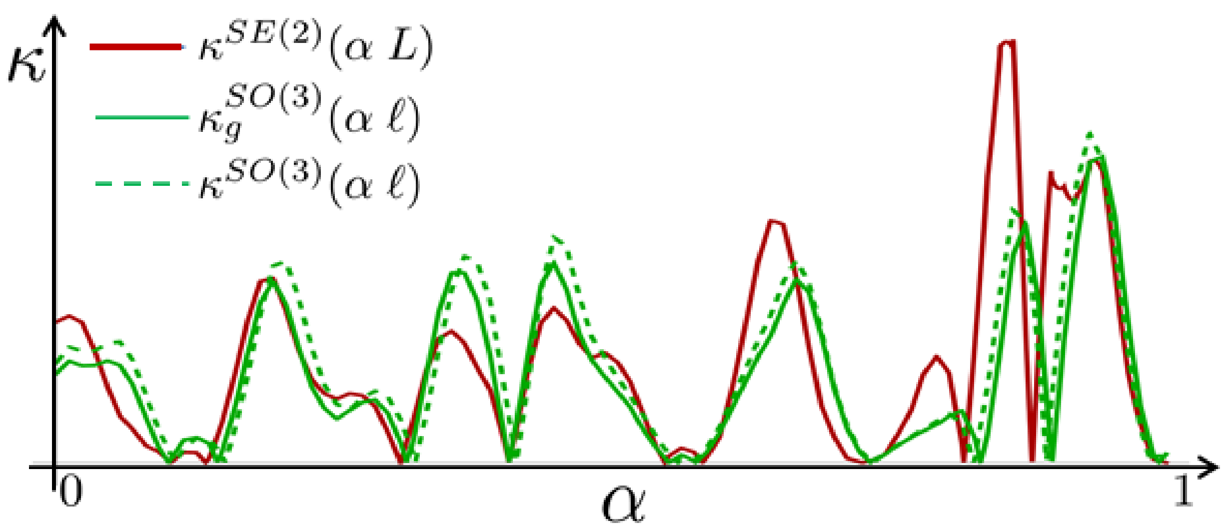

Sub-Riemannian geodesics on SE(3)

Data-driven sub-Riemannian geodesics on **SE(3)** are used for detection and analysis of neuron fibers in magnetic resonance images of a human brain.

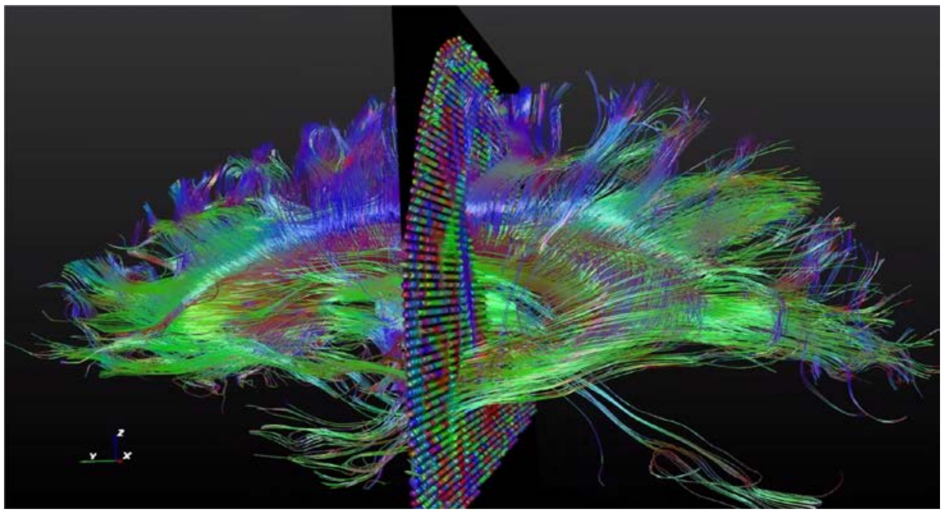

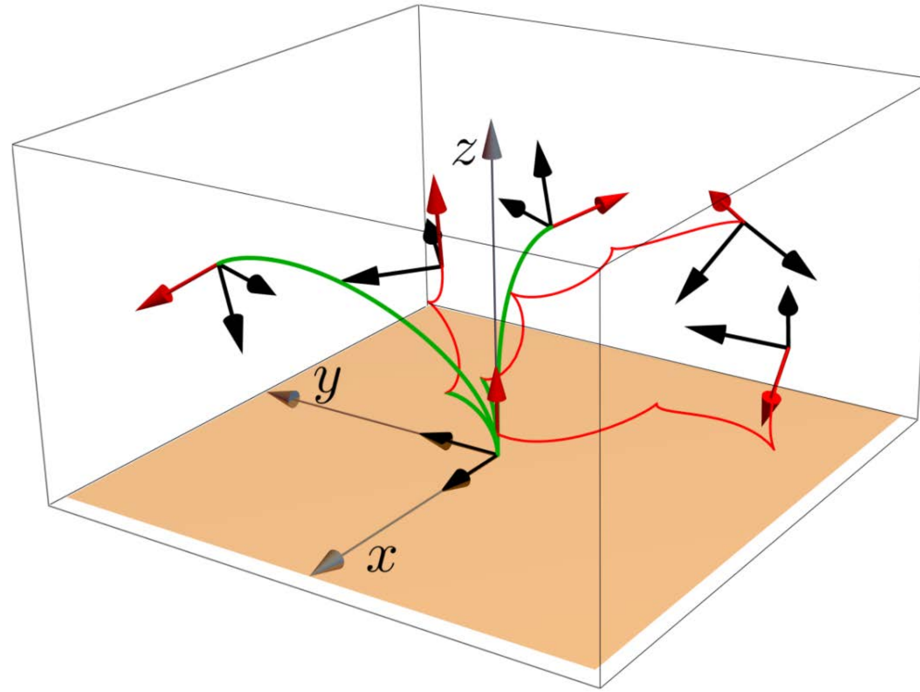

[**1**] R. Duits, A. Ghosh, T. Dela Haije, A. Mashtakov, *On sub-Riemannian geodesics in SE(3) whose spatial projections do not have cusps*, JDCS, 2016.

[**2**] A. Mashtakov, A. Popov *Extremal Controls in the Sub-Riemannian Problem on the Group of Motions of Euclidean Space*, RCD, 2017.

Sub-Riemannian Fast Marching in SE(3)

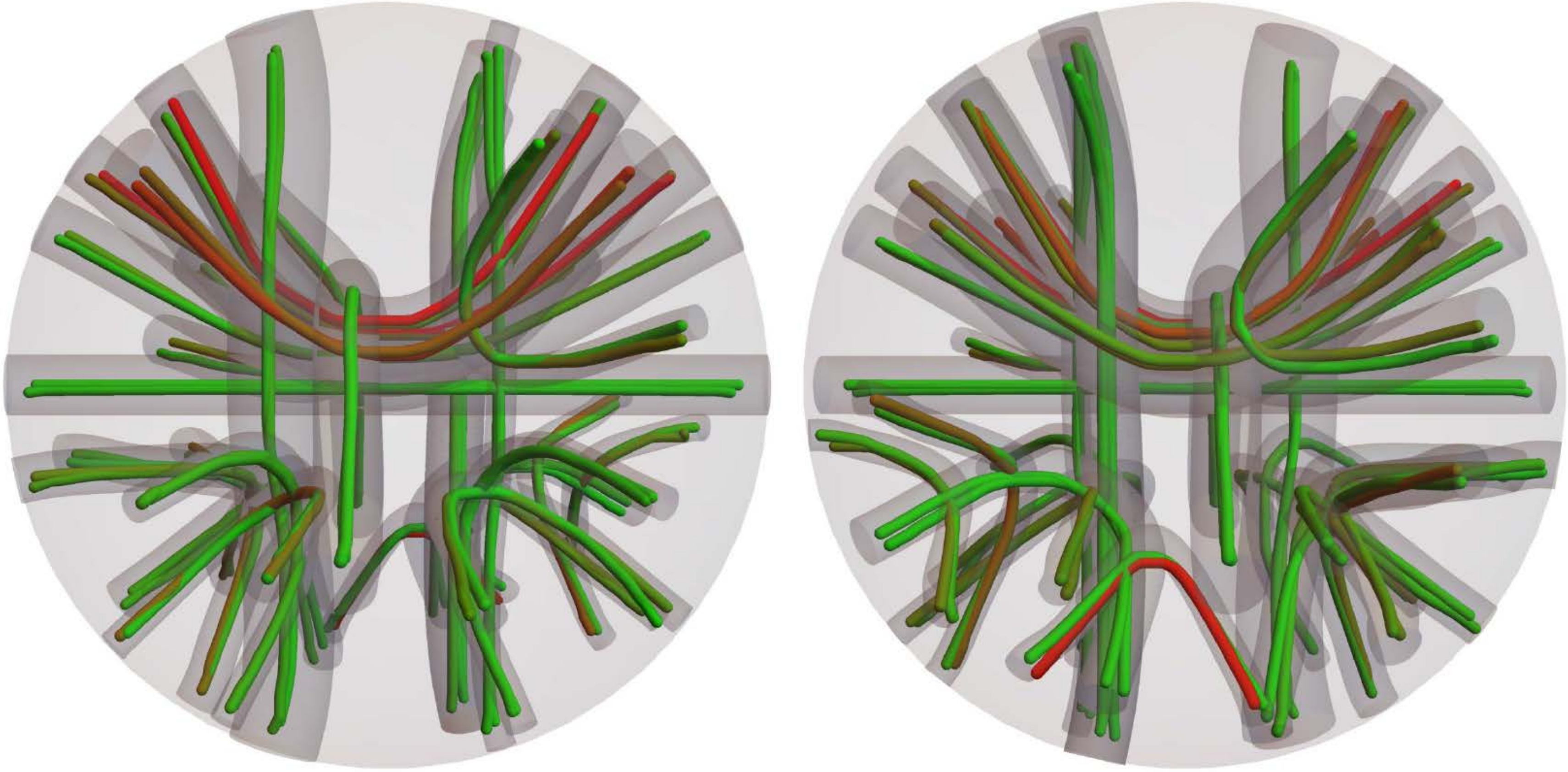

Replicated from J. Portegies, S. Meesters, P. Ossenblok, A. Fuster, L. Florack, R. Duits. Brain Connectivity Measures via Direct Sub-Finslerian Front Propagation on the 5 D Sphere Bundle of Positions and Directions, MICCAI, 2018.

Data-driven Sub-Riemannian Geodesics on SE(2) for Modelling of Geometrical Optical Illusions

Geometrical Optical Illusions

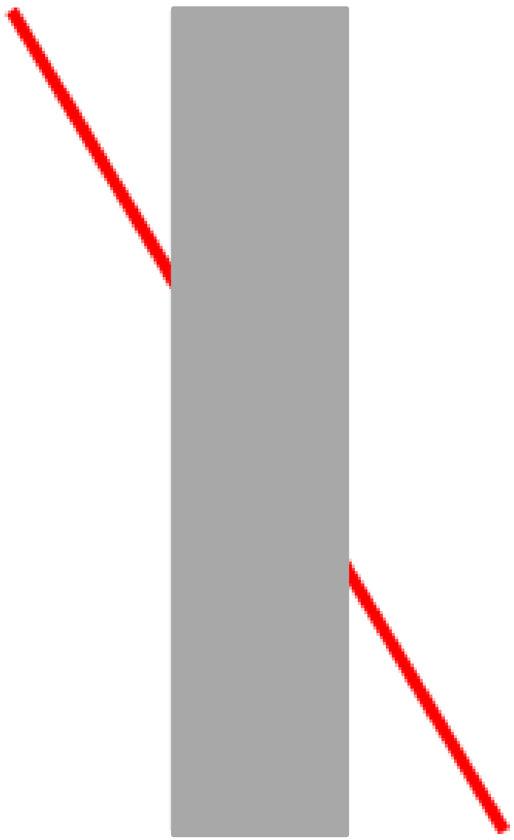

Poggendorff illusion

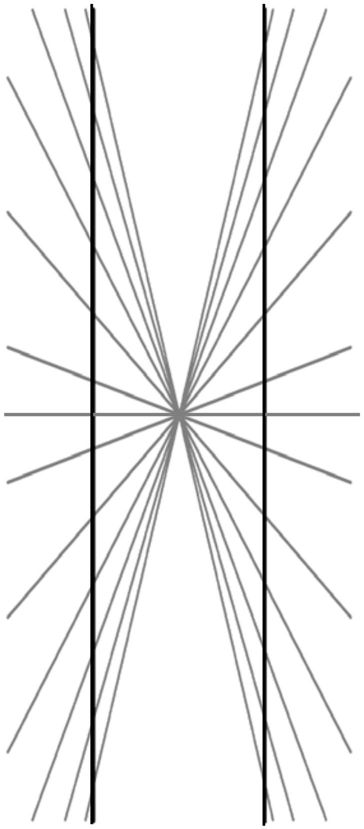

Hering illusion

Geometrical Optical Illusions

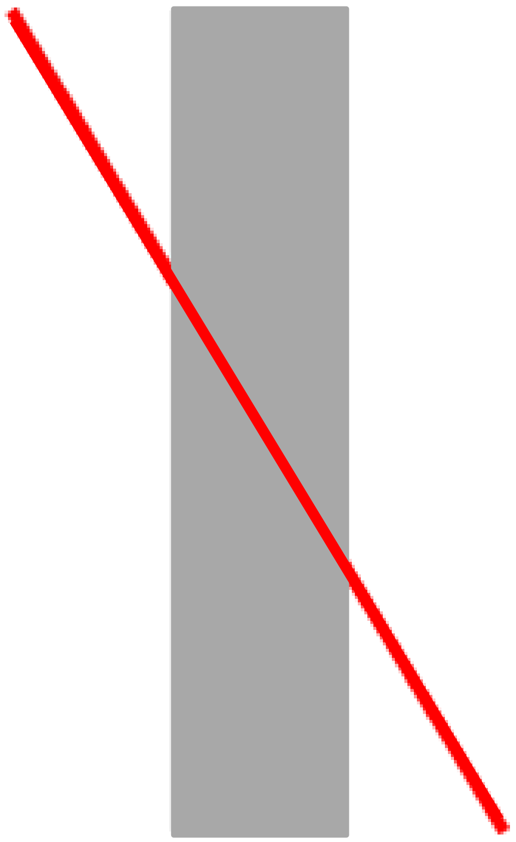

Poggendorff illusion

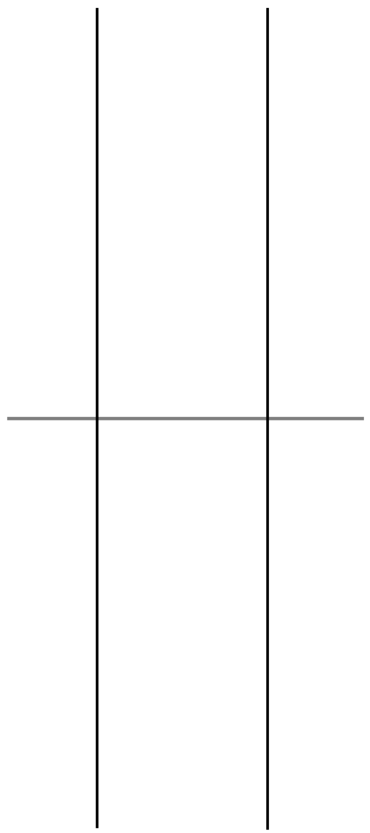

Hering illusion

Modelling of Illusory Contour

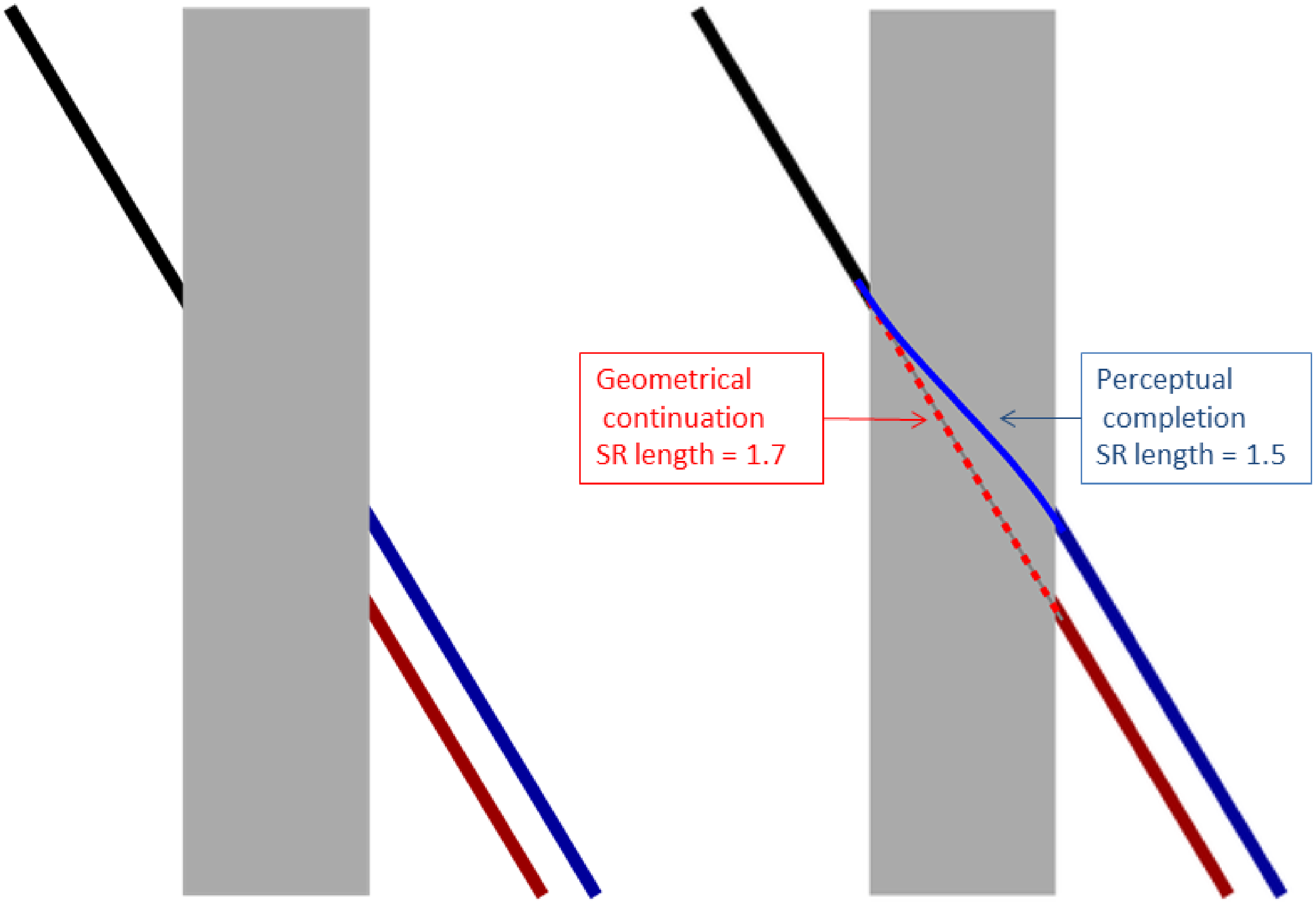

Idea: The illusory contour appears as a geodesic in a metric induced by visual stimulus.

GOIs via data-adaptive SR geodesics

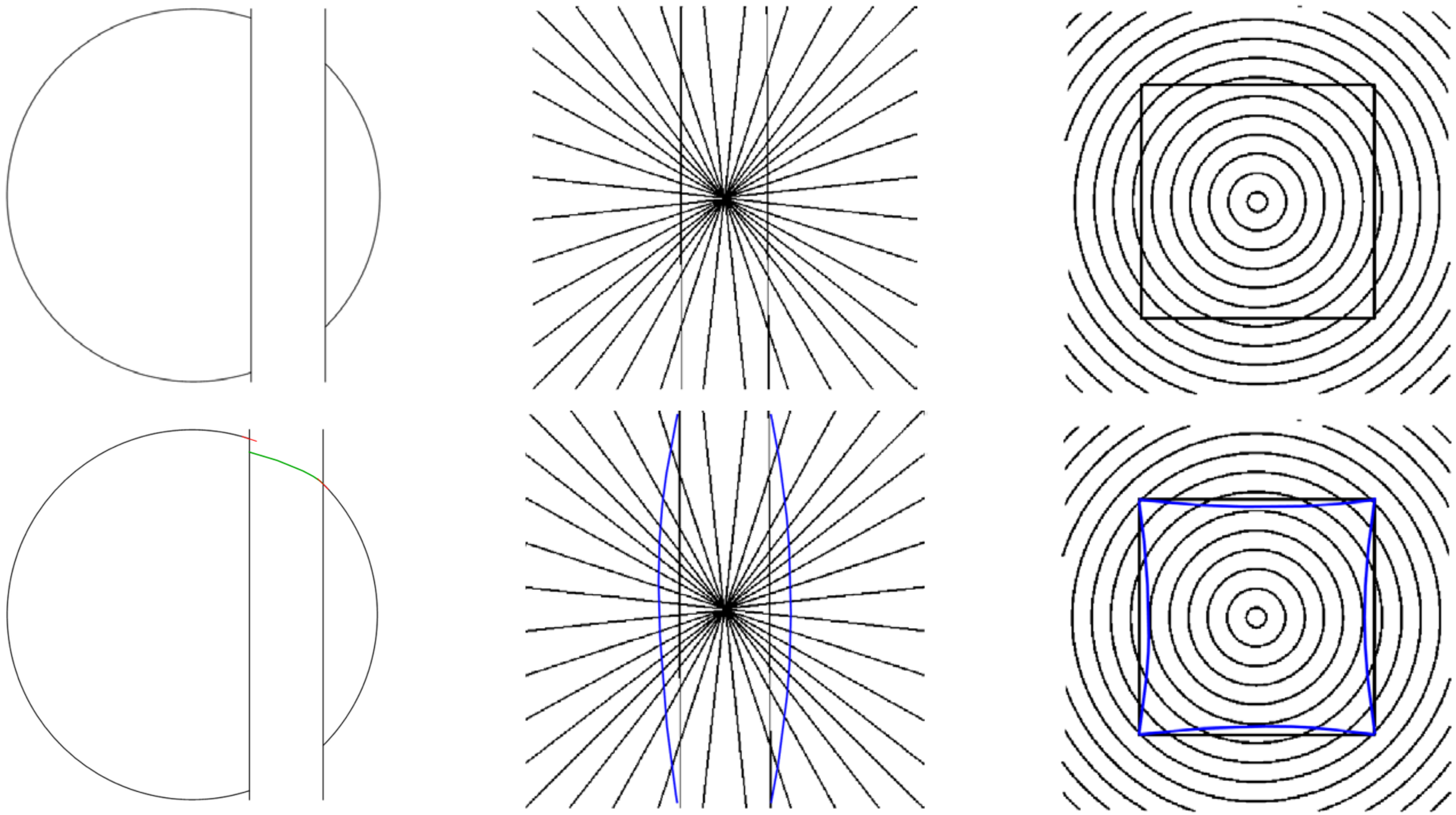

[**1**] B. Franceschiello, A. Mashtakov, G. Citti, A. Sarti, *Modelling of the Poggendorff Illusion via Sub-Riemannian Geodesics in the Roto-Translation Group*, LNCS, 2017.
[**2**] B. Franceschiello, A. Mashtakov, G. Citti, A. Sarti, *Geometrical optical illusion via sub-Riemannian geodesics in the roto-translation Group*, DGA, 2019.

Construction of External Cost

Retinal Plane $\mathbb{R}^2 \ni (x, y)$. Stimulus of Intensity $I(x, y) : M \subset \mathbb{R}^2 \to \mathbb{R}^+$.

Local coordinates $\chi = (\chi_1, \chi_2) \in M$ centered at (x, y).

Gabor Filters:

$$\psi_0(\chi) = \psi_0(\chi_1, \chi_2) = \frac{\alpha}{2\pi\sigma^2} e^{\frac{-(\chi_1^2+\alpha^2\chi_2^2)}{2\sigma^2}} e^{\frac{2i\chi_2}{\lambda}},$$

$\lambda > 0$ spatial wavelength, $\alpha > 0$ spatial aspect ratio, $\sigma > 0$ deviation.

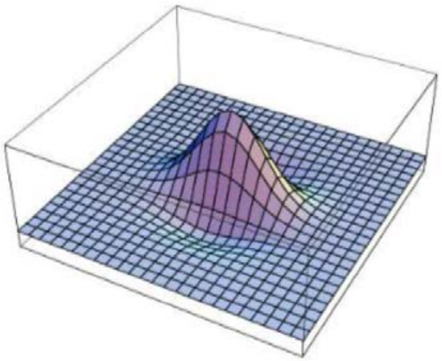

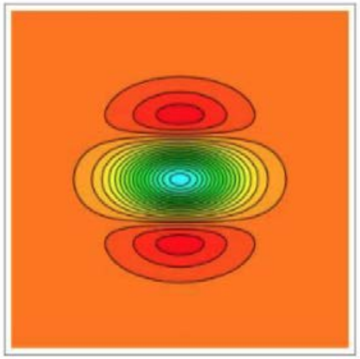

Even part

$$\mathrm{Re}(\psi_0(\chi)) = \frac{\alpha}{2\pi\sigma^2} e^{\frac{-(\chi_1^2+\alpha^2\chi_2^2)}{2\sigma^2}} \cos \frac{2\chi_2}{\lambda}$$

detection of contours.

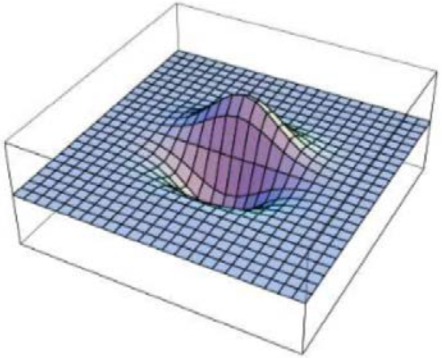

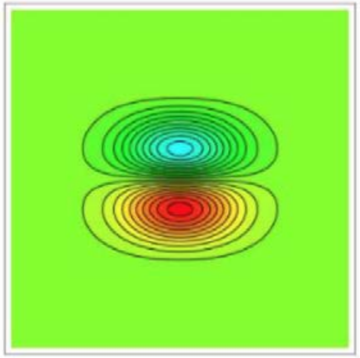

Odd part

$$\mathrm{Im}(\psi_0(\chi)) = \frac{\alpha}{2\pi\sigma^2} e^{\frac{-(\chi_1^2+\alpha^2\chi_2^2)}{2\sigma^2}} \sin \frac{2\chi_2}{\lambda}$$

detection of boundaries.

Simulation of Illusory Contour

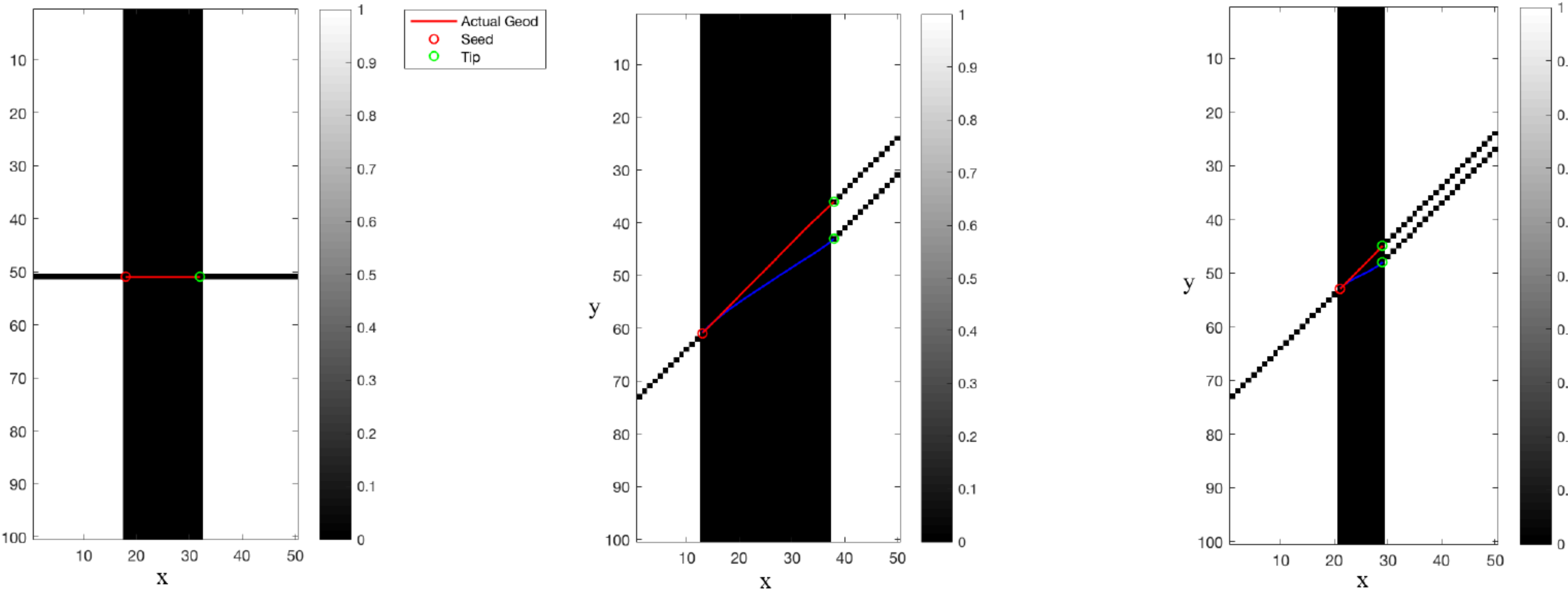

Type of curve	Width = 9 pixels	Width = 15 pixels	Width = 25 pixels
Percep. curve $\theta = \pi/4$	1.0366	1.8094	3.1113
Actual curve $\theta = \pi/4$	1.1369	2.0480	3.5354
Percep. curve $\theta = \pi/10$	2.1033	3.4719	4.9411
Actual curve $\theta = \pi/10$	2.8925	4.4927	7.3924
Percep. curve $\theta = \pi/2$	1.0320	1.4412	2.5196

Round Poggendorff Illusion

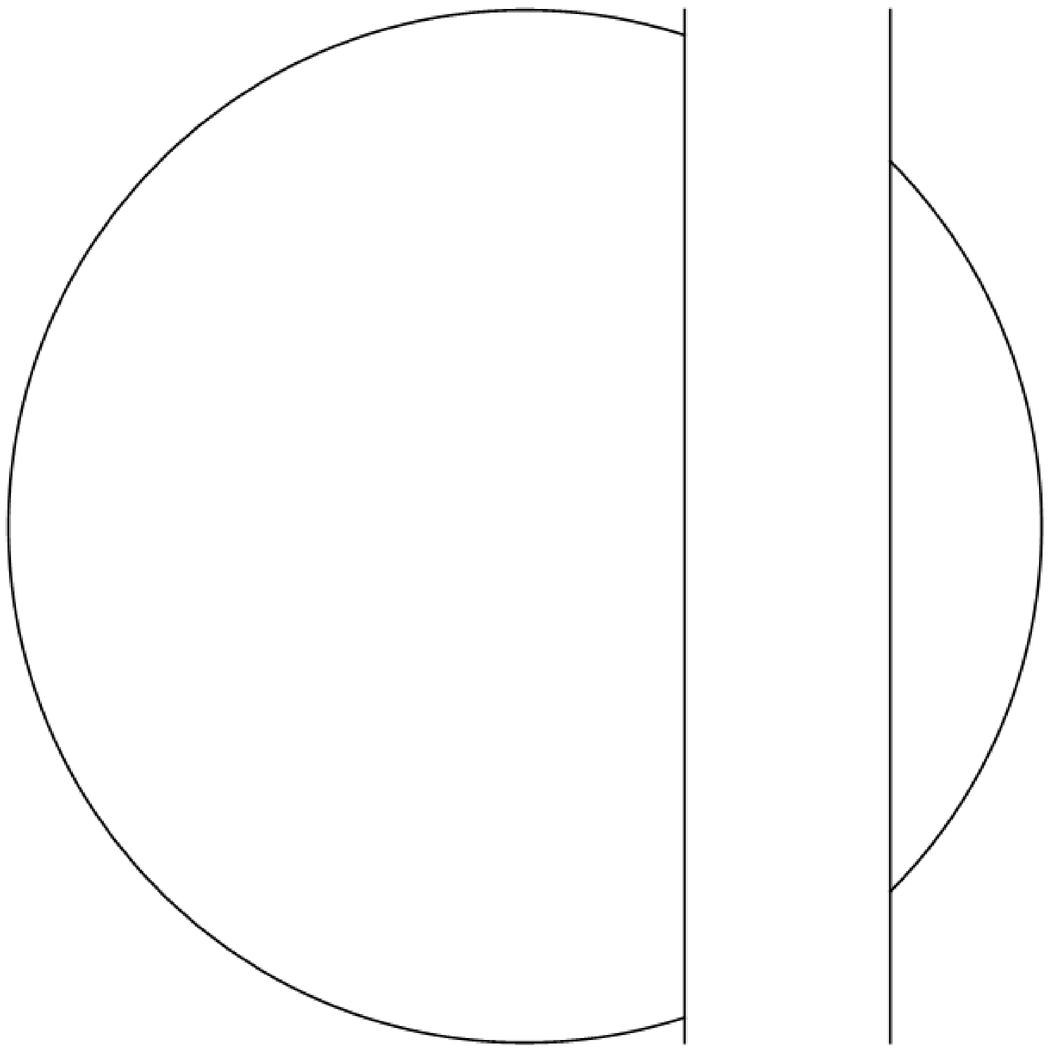

Round Poggendorff Illusion

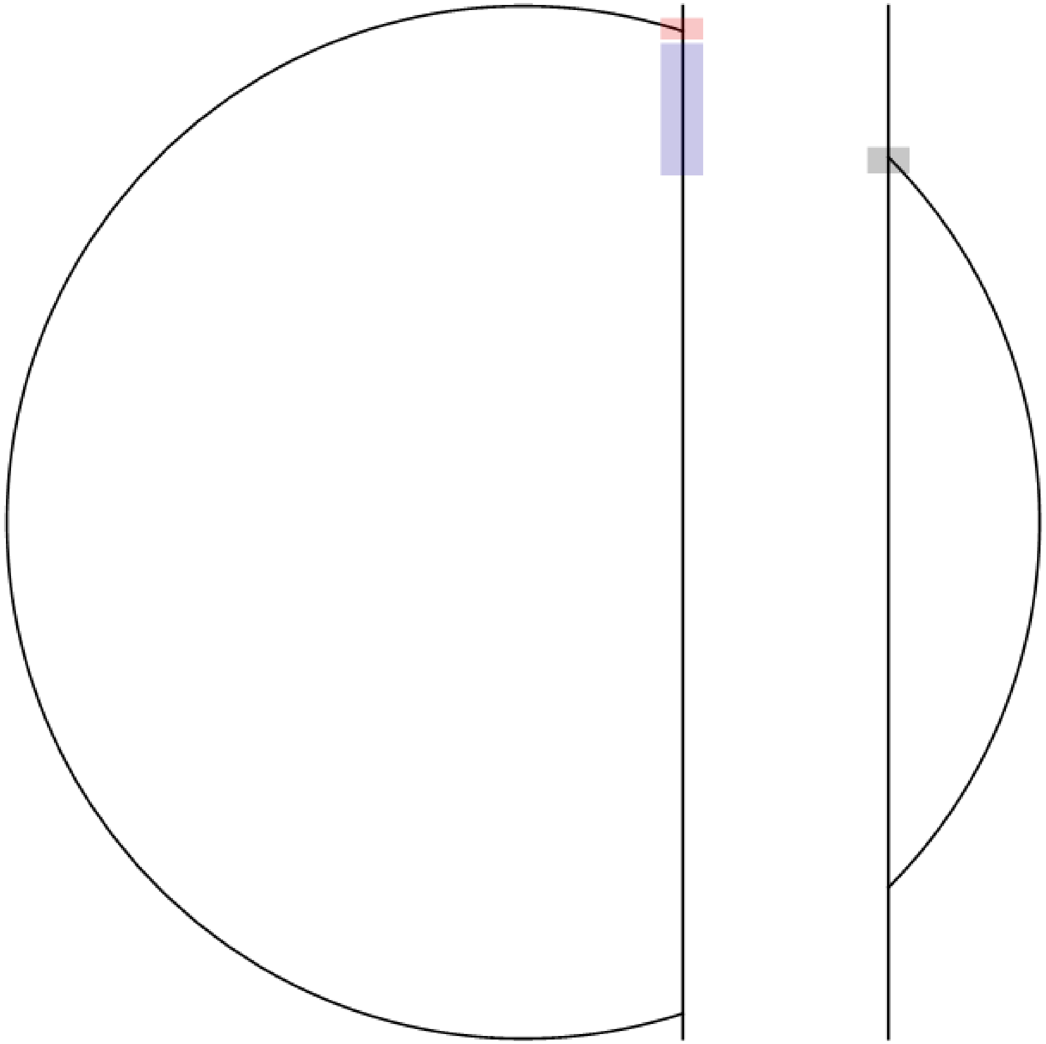

Round Poggendorff Illusion

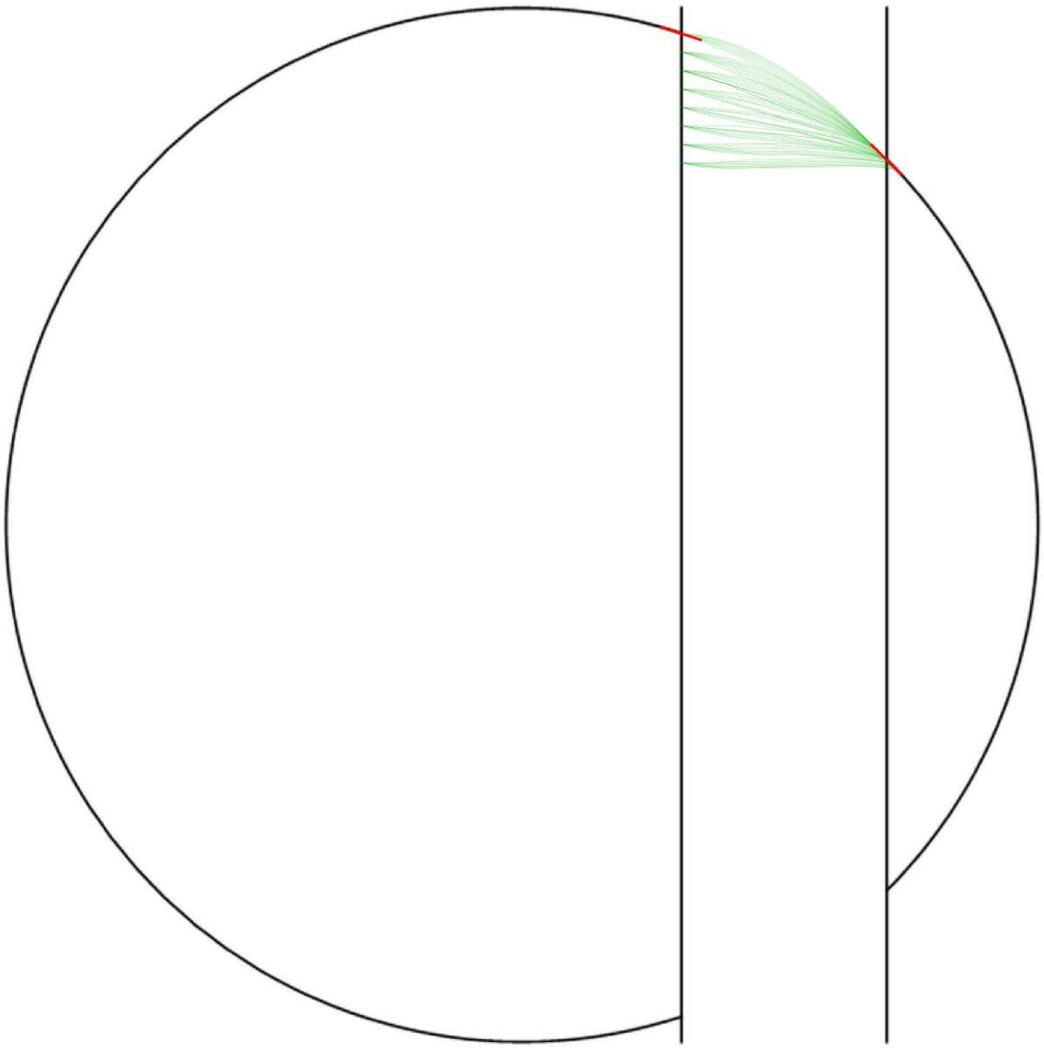

Round Poggendorff Illusion

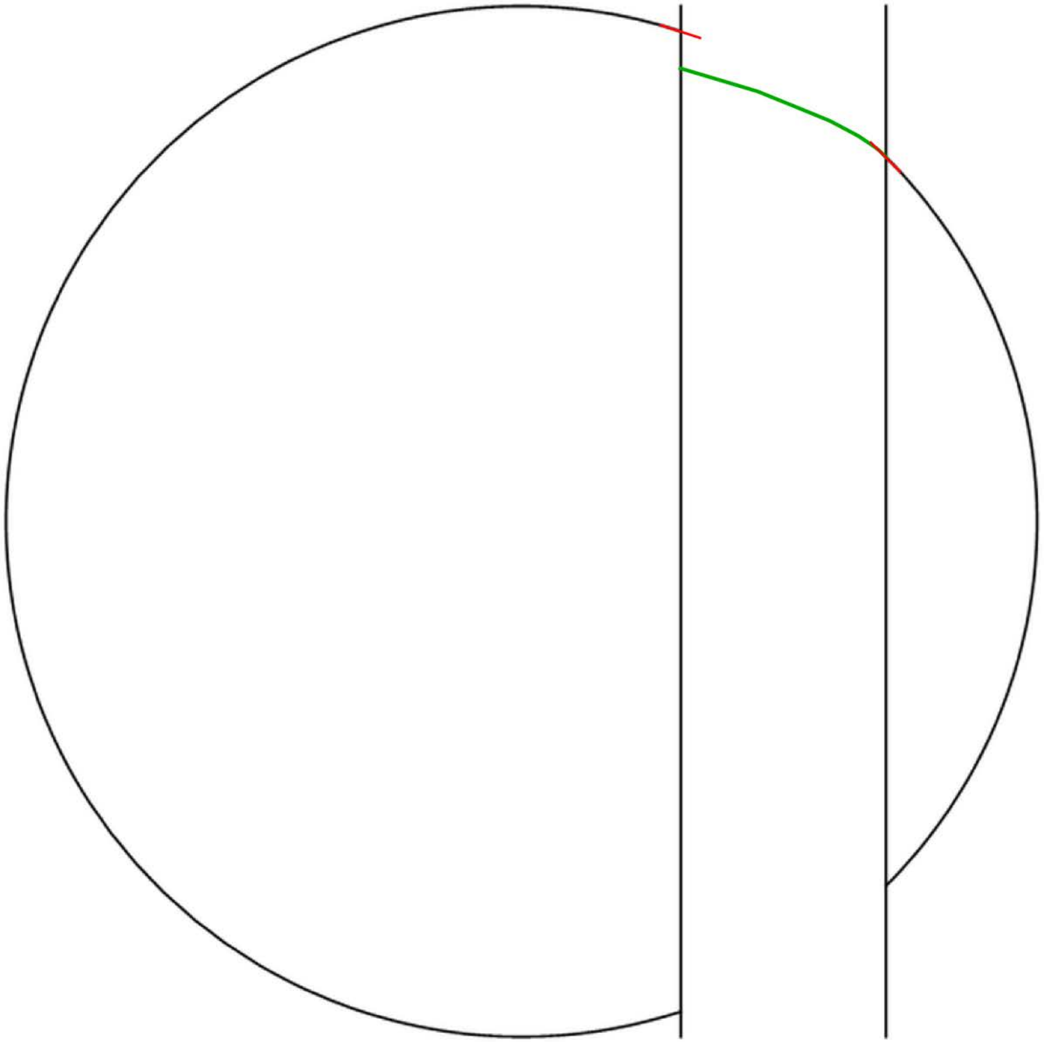

Conclusion

- Sub-Riemannian geometry is a natural tool for brain inspired image processing.
- It is used for athropomorphic image reconstruction.
- And for detection of salient lines and elongated structures in 2D and 3D images.
- Data-driven SR geodesics in SE(2) show promissing results for vessel tracking in flat images of the retina.
- In SO(3) --- in spherical images of the retina.
- In SE(3) --- for fiber tracking in 3D MRI images of human brain.
- Including data-adaptivity refines the model of V1 and explains phonomena of GOI

Thank you for your attention!